PHD3 controls energy homeostasis and exercise capacity

Haejin Yoon[1], Jessica B. Spinelli[1], Elma Zaganjor[1], Samantha J. Wong[1], Natalie J. German[1], Elizabeth C. Randall [2], Afsah Dean[3], Allen Clermont[3], Joao A. Paulo[1], Daniel Garcia[4], Hao Li[5], Nathalie Y. R. Agar[2, 6, 7], Laurie J. Goodyear[3], Reuben J. Shaw[4], Steven P. Gygi[1], Johan Auwerx[5], Marcia C. Haigis[1*]

[1]Department of Cell Biology, Harvard Medical School, Boston, [2]Department of Radiology, Brigham and Women's Hospital, Harvard Medical School, Boston, Boston, [3]Section on Integrative Physiology and Metabolism, Joslin Diabetes Center, Boston, [4]The Salk Institute for Biological Studies, 10010 N. Torrey Pines Road, La Jolla, [5]Laboratory of Integrative and Systems Physiology, École Polytechnique Fédérale de Lausanne, Lausanne 1015, Switzerland, [6]Department of Neurosurgery, Brigham and Women's Hospital, Harvard Medical School, Boston, Department of Cancer Biology, [7]Dana-Farber Cancer Institute, Harvard Medical School, Boston.

*Correspondence to Marcia_haigis@hms.harvard.edu

SUMMARY

Rapid alterations in cellular metabolism allow tissues to maintain homeostasis during changes in energy availability. Acetyl-CoA carboxylase 2 (ACC2) provides a central regulation and is phosphorylated acutely by AMPK during cellular stress to relieve repression of fat oxidation. While ACC2 is hydroxlated by prolyl hydroxylase 3 (PHD3), the physiological consequence of its hydroxylation is little understood. We find that ACC2 phosphorylation and hydroxylation occur in a reciprocal fashion. PHD3 hydroxylation occurs in conditions of high energy, leads to decreased fatty acid oxidation. Moreover, AMPK-mediated phosphorylation is inhibitory to the

hydroxylation of ACC on proline 450. PHD3 null mice demonstrate loss of ACC2 hydroxylation in heart and skeletal muscle and display elevated fatty acid oxidation. Physiologically, whole body or skeletal muscle-specific PHD3 loss enhanced exercise capacity during an endurance exercise challenge. In sum, these data identify PHD3 as a physiological regulator of energy balance during acute stress.

INTRODUCTION

Metabolic adaptation plays a fundamental role in maintaining energy homeostasis. In many tissues, fatty acids are exploited as an adaptive fuel to enable survival under conditions of metabolic stress, such as nutrient deprivation or exercise (Galgani and Ravussin, 2008; Woods and Ramsay, 2011; Palm and Thompson, 2017; Efeyan et al., 2015). Specifically, cells utilize fatty acid oxidation (FAO) to respond to low energy conditions, cold temperature, oxidative stress, and exercise (Lee et al., 2016; Chouchani et al., 2016; Grunt, 2018; Herzig and Shaw, 2018). However, the mechanism for the dynamic regulation of fatty acid oxidation in response to metabolic stress is not completely understood.

A reduction in cellular ATP and increase in the AMP/ATP ratio leads to activation of AMP-activated protein kinase (AMPK) (Hardie et al., 2012; Gowans and Hardie, 2014). In response to high AMP/ATP, AMPK phosphorylates acetyl-CoA carborylase (ACC) 1/2. AMPK phosphorylation of ACC 1/2 inhibits its activity to convert acetyl-CoA into malonyl-CoA. In the cytosol, ACC1 generates pools of malonyl-CoA for de novo lipogenesis, while ACC2 associated with the outer mitochondrial membrane generates malonyl-CoA to inhibit carnitine palmitoyltransferase 1 (CPT1), which mediates the first step of long chain fatty acid transport into the mitochondria. Thus, ACC2 phosphorylation by AMPK provides an readout of cellular energy/stress with direct ties to fat synthesis and oxidation.

ACC2 is also subject to positive regulation in the control of fatty acid metabolism via hydroxylation on P450 by proline hydroxylase domain protein 3 (PHD3) (German et al., 2016). Prolyl hydroxylase domain family members (PHDs, also called EGLN1-3) are alpha-ketoglutarate-dependent dioxygenases (REF). A previous study by German and coworkers showed that tumors with low PHD3 exhibited decreased ACC2 hydroxylation and elevated fatty

acid oxidation (German et al., 2016). By contrast, the physiological consequence of PHD3-mediated hydroxylation of ACC2 has not been examined.

Here, we reveal that PHD3 acutely hydroxylates ACC2 at proline 450 physiologically in response to nutrient and energy availability using cells, whole body PHD3 KO mice and skeletal muscle-specific PHD3 KO mice. Moreover, AMPK-mediated phosphorylation of ACC2 inhibits PHD3 binding and hydroxylation of ACC2, demonstrating one mechanism for the reciprocal relationship between ACC2 hydroxylation and phosphorylation. Using whole body or muscle specific PHD3 null mice, we probe the physiological relevance of PHD3 during fasting and exercise challenges. PHD3 is requisite for ACC2 hydroxylation in vivo and the loss of PHD3 is sufficient to increase exercise capacity. Together, these results place PHD3 and AMPK in a physiologically important signaling circuit of ACC2 hydroxylation and phosphorylation to toggle fatty acid oxidation in response to energy state.

RESULTS

ACC2 hydroxylation is negatively regulated by AMPK

In this study we sought to identify physiological conditions when PHD3 hydroxylation of ACC2 would be relevant in cells and tissues. While both PHD3 and ACC2 converge on ACC2 through distinct post-translational modifications (PTMs), whether these PTMs act in a concerted manner to regulate ACC2 activity has not been explored (Figure 1A). As PHD3 would be active under high alpha-ketoglutarate conditions, which would subsequently repress FAO, we reasoned that PHD3 would hydroxylate ACC2 in response to nutrient availability. To examine whether PHD3 activity was sensitive to fluctuations in nutrient availability, we probed ACC2 hydroxylation in mouse embryonic fibroblasts (MEFs) cultured in the presence of low (5 mM glucose) or high glucose (25 mM glucose) in the presence of 10% FBS (Figure 1B). Since AMPK senses an increased AMP/ATP ratio due to energy stress conditions, we utilized low glucose culture media as a control (Salt et al., 1998; Laderoute et al., 2006). As expected, ACC2 phosphorylation was increased in the low glucose condition, whereas, ACC2 hydroxylation was decreased (Figure 1B and 1C). Importantly, the addition of 25 mM glucose caused ACC2 hydroxylation within 5 minutes, but not in cells treated with the PHD inhibitor dimethyloxallyl glycine (DMOG) (Figure 1B and 1C). DMOG treatment significantly decreased hydroxyl ACC2

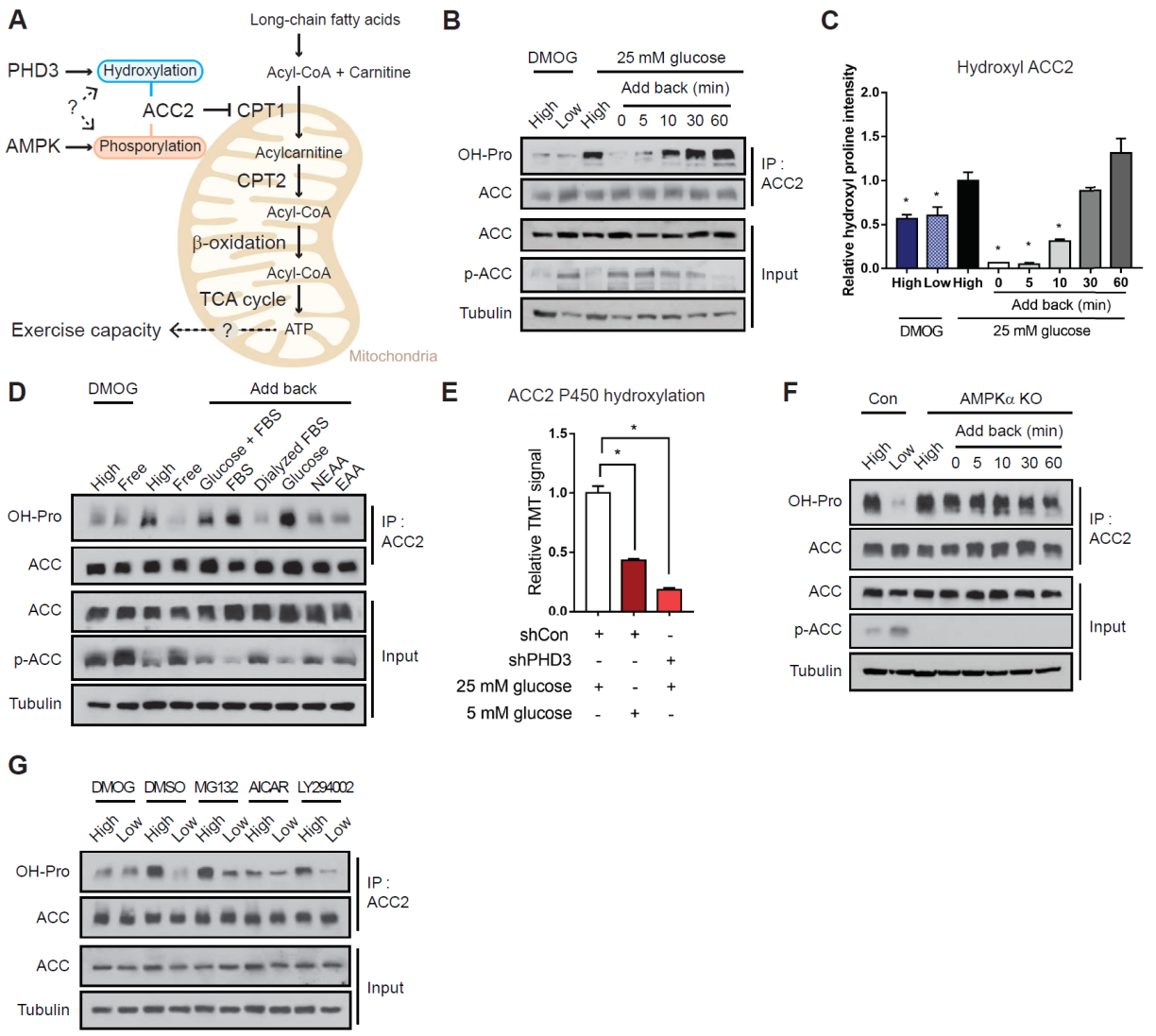

Figure 1. ACC2 hydroxylation is energy-sensitive and negatively regulated by AMPK.
(A) Schematic of fates of post-translational modification on ACC2. (B) Immunoblots of anti-ACC2 immunoprecipates and corresponding whole-cell lysates of MEFs. MEFs were grown either in high (25 mM) or low (5 mM) glucose media for 12 hr with or without PHD inhibitor DMOG (1 mM). (C) Quantitation of western blotting of (B). Hydroxyl ACC2 was normalized to total bound ACC levels. The ratio of hydroxyl ACC2: total ACC2 was normalized to respective tubulin level (n=3). (D) ACC2 hydroxylation in MEFs in high versus low glucose, and in the indicated fuel. DMOG, 1 mM Dimethyloxallyl glycine; High, 25 mM glucose with serum; -Glu/-FBS, no glucose without serum; Glucose+FBS, 25 mM glucose with serum; FBS, no glucose with serum;Dialyzed FBS, no glucose with dialyzed FBS; Glucose, 25 mM glucose without serum; NEAA, no glucose with 1% non essential amino acids; EAA, no glucose with 1% essential amino acid. (E) Representative TMT signals identifying hydroxylated P450 on ACC2 in 293T cells in control (white), 5 mM glucose media (dark red) or PHD3 knockdown cells (red). (F) Immunoblots of ACC2 hydroxylation from control or AMPKα knock out MEFs in high versus low glucose, and upon 25 mM glucose re-addition (0, 5, 10, 30 and 60 min). (G) ACC2 hydroxylation in MEFs in high or low glucose, in the presence of DMOG (1 mM for 1 h), DMSO, MG132 (10 mM for 1 h), AICAR (1 mM for 1 h) and LY294002 (50 mM for 1 h).

levels compared to the non-treated control group with high glucose media (blue and black bar) (Figure 1B and 1C). Finally, we tested whether other energetic inputs affected ACC2 hydroxylation (Figure S1A). In contrast to glucose, the addition of amino acids, fatty acids or dialyzed serum resulted in little to no induction of ACC2 hydroxylation (Figure 1D, Figure S1B-C). In sum, the rapid increase in PHD3-mediated hydroxylation of ACC2 demonstrates that PHD3 activity is acutely sensitive to glucose abundance.

To quantify in an unbiased manner which proline (P) residues on ACC2 were hydroxylated by PHD3 or regulated in response to energy stress, we analyzed ACC2 peptides from ACC2 immunoprecipitates using Tandem Mass Tag (TMT) mass spectrometry (Paulo, 2016; Navarrete-Perea et al., 2018; Berberich et al., 2018). We monitored the levels of hydroxyproline on ACC2 residue P450 by a +15.9949 Th shift (Figure S1D). Only P450 demonstrated dynamic changes in response to PHD3 or nutrients. P450 hydroxylation was diminished 5.3-fold in PHD3 KD cells compared with control cells, and P450 hydroxylation was reduced 2.3-fold in wildtype control cells cultured in low glucose compared with high glucose media (Figure 1E, Figure S1E-G). These data are consistent with the fold-changes observed in ACC2 hydroxylation detected by Western blotting (Figure S1H).

Of note, our studies demonstrate that ACC2 was phosphorylated in a reciprocal manner to its hydroxylation (Figure 1D). This observation suggested some level of circuitry between AMPK and PHD3 activity, and so we aimed to understand whether AMPK influenced PHD3 activity or vise versa. First, we tested whether PHD3 activity was affected by AMPK loss of function by measuring ACC2 hydroxylation in MEFs lacking the alpha catalytic subunit of AMPK (Figure 1F). Strikingly, the loss of AMPKα led to constitutive hydroxylation of ACC2 in a manner that was insensitive to glucose availability (Figure 1F). Likewise, the constitutive activation of AMPK by AICAR treatment decreased ACC2 hydroxylation, suggesting that AMPK-mediated phosphorylation represses PHD3-dependent ACC2 hydroxylation (Figure S1I). PHD3 expression was unchanged by ACC2 depletion or energy stress (Figure 1B, Figure S1J-L), and the depletion of PHD3 in MEFs did not alter ACC2 protein or mRNA level. We also tested whether AMPK activity was regulated by PHD3 and found that PHD3 KD did not affect the levels or kinetics of ACC2 phosphorylation.

As a control, we investigated whether modulation of other energy or nutrient sensing signaling pathways affected ACC hydroxylation. PI3K/AKT and mTOR signaling are known to coordinate with AMPK signaling via a phosphorylation cascade (Manning and Toker, 2017; Inoki at el., 2003). Cells were treated with LY294002 (PI3K/AKT inhibitor) or MG132 (proteasome inhibitor) for 1 hour and ACC2 hydroxylation status did not significantly change compared to the DMSO control (Figure 1G). We observed that only 5-aminoimidazole-4-carboxamide ribonucleotide (AICAR) treatment, which activates AMPK, decreased hydroxyl-

ACC2 in the high glucose condition to the level observed with glucose deprivation (Figure 1~~E~~G). Taken together, these data suggest that AMPK-mediated phosphorylation of ACC2 is upstream and inhibitory to PHD3-mediated hydroxylation.

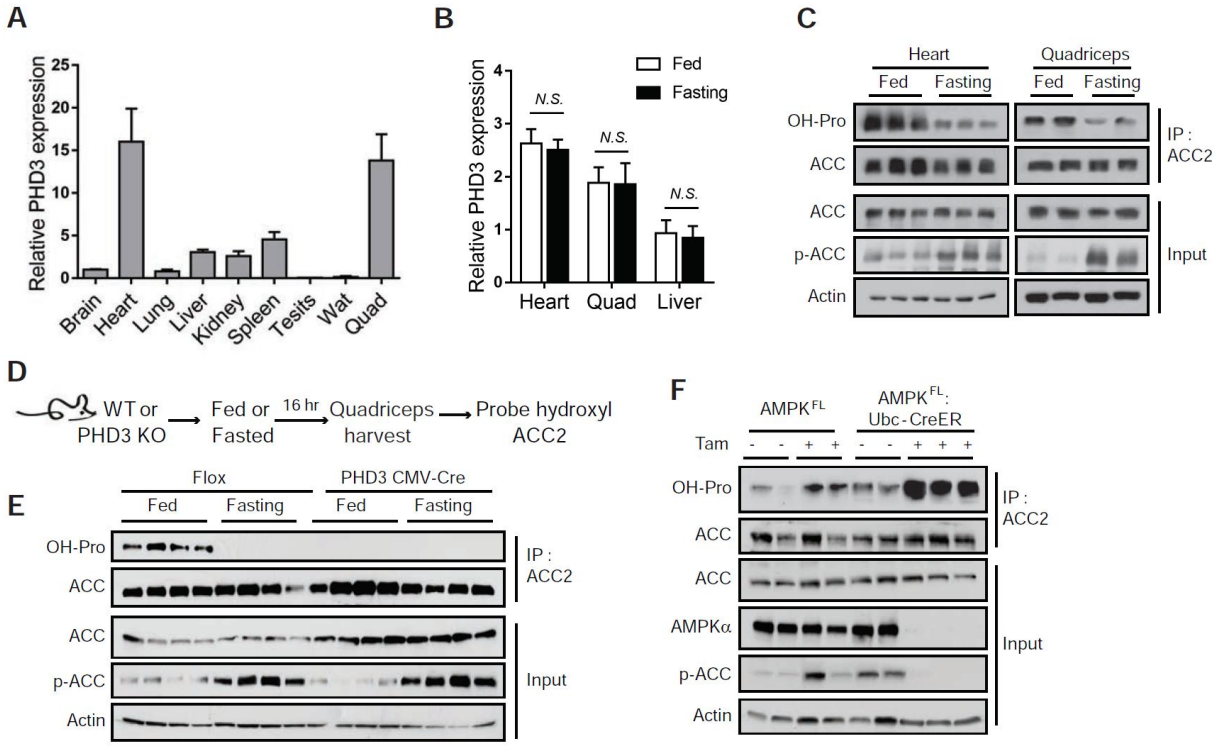

Figure 2. PHD3 has an opposite role with AMPK in metabolic sensitive organs on energy stress conditions.
(A) PHD3 mRNA levels in mouse brain, heart, lung, liver, kidney, spleen, testis, white adipose tissue, and quadriceps (n = 4). (B) PHD3 mRNA levels in mouse heart, quad and liver under fed or fasting conditions (n = 4). (C) Immunoprecipitation (IP) and western blot analysis of ACC hydroxylation from whole-cell lysates of mouse tissues that were fasted or fed for overnight. (D) Schematic of the detection of ACC2 hydroxylation in WT or PHD3 KO mouse quadriceps under fed or fasted condition. (E) Immunoprecipitation and western blot analysis of ACC2 hydroxylation and phosphorylation in WT or PHD3 KO mouse quadricep muscles in fed and fasted conditions, N = 4. (F) Immunoprecipitation and western blot analysis of ACC2 hydroxylation in quadriceps from AMPK-WT and AMPK-KO mice. AMPKFL;Ubc-CreER mice were treated with tamoxifen (4mg per day, for 5 days) to induce knockout of AMPK. Quadriceps were harvested 3 weeks post-tamoxifen treatment and protein was extracted.

Nutrient deprivation *in vivo* alters PHD3 activity, but not expression levels.

We then examined whether PHD3 and ACC2 hydroxylation was sensitive to changes in nutrients *in vivo*. ACC2 loss results in increased overall energy expenditure in mice, demonstrating a key role for fatty acid metabolism in physiological energy homeostasis (Choi et al., 2007). In order to activate AMPK and energy stress *in vivo*, we fasted mice for 16 hours and immunoprecipitated ACC2 from heart and quadriceps muscle to assess hydroxylation and phosphorylation. These tissues were probed because they expressed the highest levels of PHD3 compared to brain, lung, liver, kidney, spleen, testis and white adipose (Figure 2A). Although PHD3 expression was unchanged with fasting (Figure 2B), ACC2 hydroxylation was

significantly decreased in heart and quadriceps from fasted mice relative to fed mice (Figure 2C). Conversely, phosphorylated ACC2 was increased upon fasting in both tissues, consistent with elevated AMPK activity under these conditions (Figure 2C). By contrast, PHD3 expression is low in the liver, a tissue that does not respond to fasting by inducing AMPK-mediated phosphorylation of ACC2. Likewise, we did not observe changes in ACC2 hydroxylation in liver during fasting.

To determine if PHD3 was required for ACC2 hydroxylation in vivo, we generated PHD3 knockout (KO) mice (Figure S2A-C) (Takeda et al., 2006). PHD3 was requisite for hydroxylation of ACC2 (Figure 2D) in quadriceps muscle, demonstrating that PHD3 hydroxylates ACC2 *in vivo* (Figure 2E). Importantly, loss of PHD3 did not affect ACC2 phosphorylation, consistent with cellular data that PHD3 activity does not act upstream of AMPK (Figure 2E). To determine if AMPK regulates PHD3 function *in vivo*, we measured ACC2 hydroxylation in AMPKα KO mice. $AMPK^{FL}$-Ubc-Cre^{ER} (AMPKα KO) mice were treated with 4 mg of tamoxifen for 5 days to knockout AMPK, and ACC2 hydroxylation was probed in AMPKα KO mice quadriceps (Figure 2F). As expected, ACC2 was not phosphorylated in these animals due to loss of AMPK catalytic activity (Figure 2F). Consistent will cellular data, loss of AMPK activity *in vivo* increased ACC2 hydroxylation compared to control mice (Figure 2F). Taken together, these findings demonstrate that PHD3 is required for ACC2 hydroxylation in vivo and that levels of ACC2 hydroxylation are sensitive to the energy status of tissues.

ACC2 and PHD3 binding is interrupted by serine 222 phosphorylation.

As ACC2 has been shown to physically bind with PHD3 (Tran et al., 2015; German et al., 2016), we sought to elucidate whether this binding was sensitive to cellular nutrient status. ACC2 is a 280-kDa multi-domain enzyme, comprised of: N-terminal (NT), biotin carboxylase (BC), carboxyltransferase (CT), and biotin carboxyl carrier protein (BCCP) (Figure 3A, Figure S3A-B) (Tran et al., 2015; Tong et al., 2006). ACC2 residues S222 and P450 reside in the NT and BC domains, respectively (Figure 3A, Figure S3A), which are modeled to form a dimer with an interface adjacent to S222 phosphorylation sites, whereas P450 resides on the outside of the dimer interface (Figure 3A). We engineered 293T cells to express C-terminal-Flag-tagged ACC2

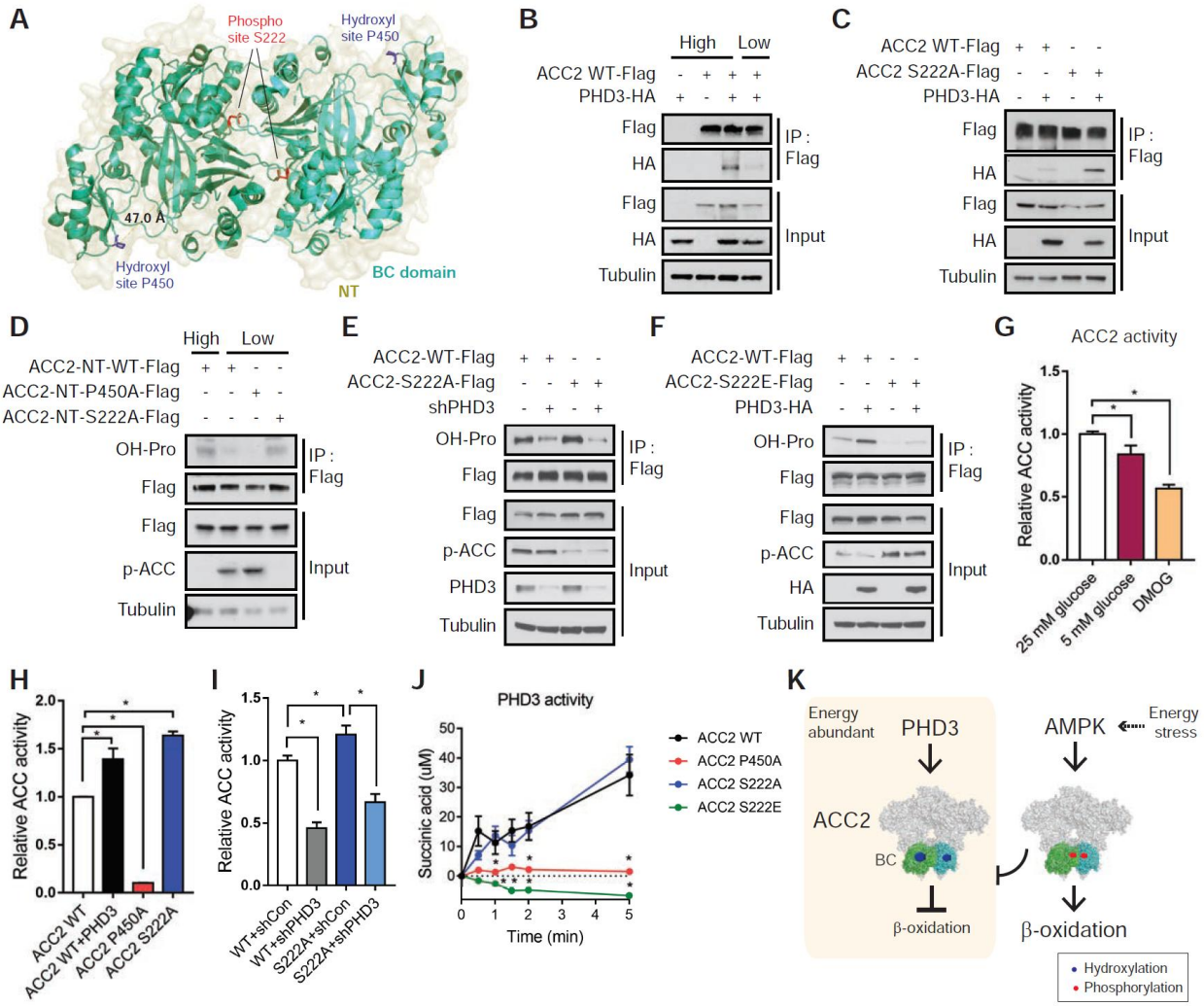

Figure 3. ACC2 P450A mutants functianally phenocapies hyperactive AMPK.
(A) P450 (hydroxylation site, blue) is located in the ACC2 BC domain (green and cyan, PDB: 3JRW). The distance between S222 (phosphorylation site, red) and hydroxylation sites is approximately 47 Å. (B) HEK293T cells were transfected with ACC2-Flag and/or PHD3-HA. Cells were incubated with 25 mM high glucose media or 5 mM low nutrient media for 8 h. Proteins in cell lysates were precipitated by anti-Flag antibody and immunoblotted using the indicated antibodies. (C) IP and western blot analysis of PHD3 and ACC2 interaction in the presence or absence of S222A mutation on ACC2. (D) Phosphorylation of ACC2 interrupts the binding between ACC2 and PHD3. ACC2 N-terminus (NT)-WT-Flag, ACC2 NT-P450A-Flag, ACC2 NT-S222A-Flag and/or PHD3-HA were transfected into HEK293T cells. Proteins were immunoblotted using the indicated antibodies. (E) IP and western blot analysis of ACC2 hydroxylation in HEK293T cell lines with overexpression of WT ACC2 or ACC2 S222A with PHD3 silencing. (F) IP and western blot analysis of ACC2 hydroxylation in HEK293T cell lines with overexpression of WT ACC2 or ACC2 S222E with PHD3. (G) ACC activity assay in HEK293T cell lines in 25 mM glucose (high nutrient), 5 mM glucose (low nutrient), or DMOG. Activity was normalized to protein level (n=4). (H) ACC activity assay in MEFs overexpressing WT ACC2, ACC2 P450A, ACC2 S222A or PHD3 (n = 3). (I) ACC activity assay in MEFs overexpressing WT ACC2, ACC2 P450A, ACC2 S222A, or PHD3 (n=4). (I) ACC2 activity assay in MEFs overexpressed ACC2 WT or ACC2 S222A with PHD3 silencing. (J) *In vitro* hydroxylation assay for PHD3 enzymatic activity with recombinant protein about N-terminus domains of ACC2 WT, ACC2 P450A, S222A, or S222E, and PHD3 (n=3). (K) Schematic figure that AMPK-induced phosphorylation inhibits PHD3-related hydroxylation on ACC2 dimer structure. Posttranslational modifications by AMPK (red dots) and PHD3 (blue dots) on the ACC2 BC domain are indicated in the estimated ACC2 model (PDB: 5CSL).

and C-terminal-HA-tagged PHD3. WT-PHD3 and WT-ACC2 co-immunoprecipitated in cells cultured in high glucose compared but not in low glucose (Figure 3B), demonstrating that this binding was nutrient sensitive. As AMPK reduced PHD3 activity, we tested whether ACC phosphorylation interfered with PHD3 binding by measuring the co-immunoprecipitation of PHD3-HA with WT ACC2, S222A ACC2, or S222E ACC2 in the HEK 293T. First, PHD3 co-immunoprecipitated with an S222A variant of ACC2 with greater intensity compared with WT ACC2, suggesting that phosphorylation may be inhibitory to this binding interaction (Figure 3C).

To begin to biochemically define the interaction between these proteins, we mapped the domain(s) on ACC2 important for binding to PHD3 (Figure S3C-H). Each domain was expressed recombinantly in *E. coli* with a C-terminal GST-tag, purified, and incubated *in vitro* with recombinant PHD3-HA-His to test their ability to co-immunoprecipitate. We observed that the BC domain co-immunoprecipitated with PHD3 *in vitro*, while the CT and BCCP domains demonstrated no interaction (Figure S3C-E). The reciprocal immunoprecipitation with anti-HA (Figure S3F-H) also identified selective binding between PHD3 and the BC domain (Figure S3C-I).

Our cellular and *in vivo* studies demonstrate that AMPK inhibition increased ACC2 hydroxylation, while AICAR treatment decreased hydroxylation in cells. These findings are consistent with a model that AMPK activity or phosphorylation of ACC2 may be inhibitory to PHD3. Since AMPK activity represses PHD3-mediated hydroxylation of ACC2, we tested the hypothesis that phosphorylation of S222 blocks the PHD3-ACC2 binding interaction *in vitro*. To probe the binding interaction between PHD3 and ACC2, we generated an expression construct to overexpress the N-terminal domain of WT ACC2 containing amino acids 1-763 (ACC2-NT-WT) or an AMPK phospho-mutant (ACC2-NT-S222A) in 293T cells (Figure S3B). This truncated variant encompasses the biotin carboxylase and ATP grasp domains and migrates distinctly from full length ACC (~250 kDa), allowing us to isolate the effect of each PTM. To confirm this PHD3 binding with ACC2 mutant affects hydroxylation status, we transfected WT ACC2, P450A ACC2 or S222A ACC2 into 293T cells and measured hydroxylation of ACC2 using immunoprecipitated with anti-ACC2 (Figure 3D). ACC2-NT-WT co-immunoprecipitated with PHD3 in cells and was hydroxylated (Figure 3D, Figure S3I-J). In our data using full length ACC2, we observed phosphorylation bands of full length ACC even when the ACC2 S222A mutant is overexpressed, which represents the phosphorylation of endogenous ACC1 and ACC2. ACC2 hydroxylation was decreased in low nutrient compared to high nutrient condition in ACC2-NT-WT. Also, ACC2-NT-P450 had dramatically lower hydroxylation in low nutrient condition (Figure 3D). By contrast, the constitutively dephosphorylated mutant ACC2-NT-S222A displayed increased PHD3 binding capacity and was more hydroxylated under low nutrient conditions. To confirm the phosphorylation site is important on ACC2 hydroxylation, we measured hydroxylation of ACC2 on ACC2-WT or S222A ACC2 with PHD3 silencing in 293T cells. ACC2 hydroxylation was decreased in PHD3 knock downed cells compared to

control group (Figure 3E). However, the hydroxylation was increased in S222A ACC2 but not in ACC2 WT (Figure 3E), according to the binding intensity (Figure 3C). Finally, as loss of phosphorylation increases PHD3–mediated hydroxylation of ACC2, we tested whether a mutation to mimic constitutive phosphorylation of ACC2 (S222E) diminished hydroxylation. The ACC2 S222E mutant had decreased hydroxylation levels (Figure 3F), which further supports a model whereby the phosphorylation of ACC2 inhibits PHD3-mediated hydroxylation (Figure 3F). These data suggest that loss of phosphorylation on S222 is sufficient to enhance PHD3 hydroxylation of ACC2.

Since AMPK activity repressed hydroxylation of ACC2 by PHD3, we examined how these two signaling pathways converged on ACC2 during the energy adaptation in cells during low glucose stress. First, we performed a direct biochemical assay of ACC2 activity using radioactive sodium bicarbonate on immunoprecipitated ACC2 from cells. Using this assay we found that ACC2 activity was decreased in 5 mM glucose and DMOG treatment compared to WT (Figure 3G), consistent with low glucose and DMOG inhibiting PHD3-mediated ACC2 hydroxylation. To understand the ACC2 activity is affected by PHD3-mediated hydroxylation of ACC2, we test ACC2 activity assay in ACC2 WT, P450A ACC2 or S222A ACC2 with PHD3 overexpressing 293T cells (Figure 3H). ACC2 was activated by PHD3 and lost its activity in P450A mutant, which is the hydroxylation site targeted by PHD3 (Figure 3H). Oppositely, ACC2 activity was increased in S222A ACC2 compared to ACC2 WT (Figure 3H). Also, ACC2 activity was increased by PHD3 overexpression and in ACC2 S222A mutant (no phosphorylation) conditions (Figure 3I), consistent with phosphorylation repressing ACC2 hydroxylation (Figure 3E).

To probe how the phosphorylation on S222 affects the ability of ACC2 to be hydroxylated we measured the activity of purified, recombinant PHD3 using the N-terminal domain of ACC2, P450A ACC2, S222A ACC2, or S222E ACC2 as substrates. PHD3 uses oxygen and α-ketoglutarate to hydroxylate target proline residues, generating carbon dioxide and succinate in the process. Thus, to quantify PHD3 activity, we measured the production of succinate over the course of the reaction (Figure 3J). While PHD3 demonstrated activity using WT ACC2 as a substrate, PHD3 possessed no detectible activity towards the ACC2 P450A mutant. While PHD3 showed activity using the S222A ACC2 variant, the phospho-mimetic

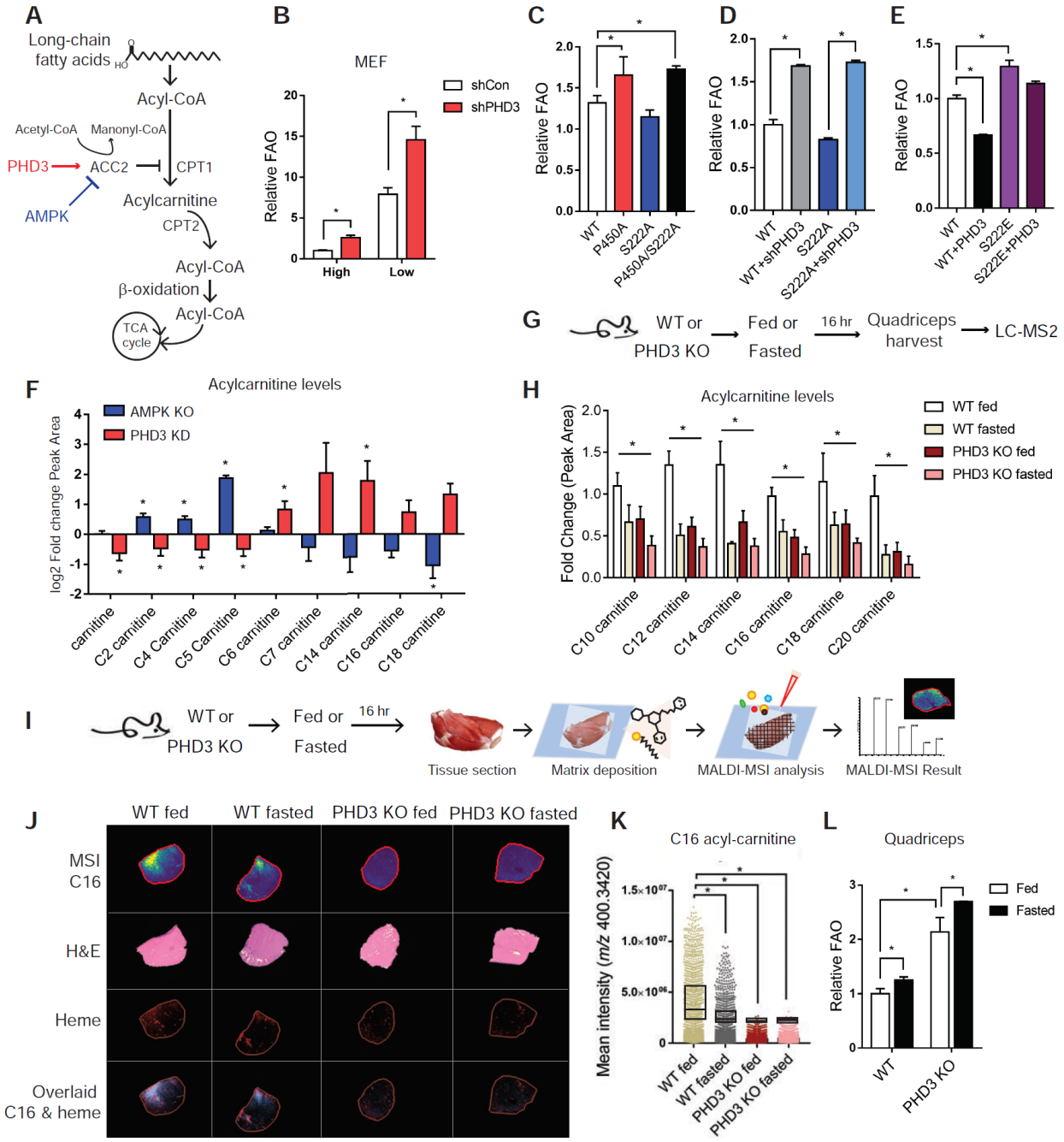

Figure 4. Loss of PHD3 results in increased fatty acid catabolism in mouse muscle.
(A) Schematic of the regulation of long chain fatty acid oxidation by PHD3 and AMPK (B) Palmitate oxidation in WT or PHD3 knockdown MEFs under high or low nutrient condition using FAO analysis (n = 3). (C) Palmitate oxidation assay in MEFs with overexpressed ACC2 WT, ACC2 P450A, ACC2 S222A or ACC2 P450A/S222A double mutant (n = 3) using FAO analysis. (D) FAO analysis in MEFs overexpressed ACC2 WT or ACC2 S222A with PHD3 silencing (n = 3). (E) Palmitate oxidation assay in MEF cell lines with overexpression ACC2 WT, S222E, or PHD3 (n=3). (F) Relative abundance of acylcarnitines in MEFs depleted of PHD3 (red) and AMPK (blue) compared to control cells. For all comparisons two-tailed t test was used. N = 4, $P < 0.05$. (G) Flowchart of the metabolomic analysis using LC-MS in WT or PHD3 KO mouse under fed or fasted condition. (H) The relative metabolite abundance of long chain acyl-carnitines in WT or PHD3 KO mouse quadriceps under fed or fasted condition (n = 4). (I) Flowchart of the metabolomics analysis in WT or PHD3 KO mouse quadriceps under fed or fasted condition. (J) Matrix-assisted laser desorption/ionization mass spectrometry imaging (MALDI-MSI) of palmitoylcarnitine (C16 acyl-carnitine, m/z 400.3420, Δ ppm = 1.16) in WT or PHD3 KO mouse quadriceps under fed or fasted conditions, alongside H&E stained serial sections. Comparison of distribution of different ions - acyl-carnitine distribution correlates with vasculature. (K) The scatter dot plot of relative abundance of palmitoyl-carnitine under each condition. (L) Palmitate oxidation in WT or PHD3 KO mice quadriceps under fed or fasted condition using 14C-labeled palmitate and CO_2 capture analysis (n=4).

S222E ACC2 variant was a poor substrate of PHD3. These data are consistent with the model that phosphorylation of ACC2 at S222 is inhibitory to PHD3-mediated hydroxylation of ACC2 (Figure 3K).

PHD3 represses fat catabolism *in vivo*

As long chain fatty acids are prepared for the multi-step process of mitochondrial import, they must be converted to acyl-carnitines by CPT1, which is inhibited by ACC2 (McCoin et al., 2015) (Figure 4A). We used biochemical FAO assay to determine the effects of ACC2 PTMs on FAO. In MEFs, low nutrient conditions lead to increased FAO, which is further exacerbated by PHD3 loss (Figure 4B). We repeated these experiments in C2C12 cells, which are mesenchymal stem cells that are classically used as an *in vitro* model of muscle cells (Millay et al., 2013). Our data shows that, in a manner similar to HEK293Ts and MEFs, fatty acid oxidation was decreased in C2C12 cells depleted of PHD3 (Figure S4A). Also, PHD3 knockdown repressed ACC2 hydroxylation (Figure S4B). These experiments performed *in vitro* corroborate our experiments performed *in vivo* on mouse quadriceps during fed or fasting condition (Figure 2E).

As ACC2 localizes to the outer mitochondrial membrane and generates malonyl CoA locally to repress fatty acid uptake and subsequent fatty acid oxidation, we examined the regulation of PHD3 by AMPK on FAO. Functionally, PHD3-mediated hydroxylation of ACC2 represses FAO (German et al., 2016) while AMPK-mediated phosphorylation of ACC2 activates FAO (Cho et al., 2010; O'Neill et al., 2014). As expected, MEFs overexpressing the ACC2 P450A mutation have significantly higher levels of FAO than ACC2 WT MEFs when cultured in the high glucose condition (red bar) (Figure 4C). Since AMPK is not activated under conditions of nutrient abundance, FAO was not significantly decreased in MEFs overexpressing the ACC2 S222A mutation compared to WT (blue bar) cells cultured in high glucose. We next generated the double inactive mutant P450A/S222A and observed that this double variant had increased FAO compared to WT (20.7%), and was similar to the P450A mutant. As expected, the S222A mutant reduced FAO compared to WT (-31.3%) (Figure 4C). This suggests the ACC2 P450A/S222A mutant acts similarly to the P450A mutant to increase FAO in the context of nutrient abundance. Next, we measured FAO and the level of ACC2 hydroxylation of ACC2 in the presence or absence of PHD3 and S222A ACC2. As expected, FAO was lower in ACC2 S222A overexpressing MEFs compared to ACC2 WT overexpressing cells (Figure 4D). FAO was increased in both ACC2 WT or S222A ACC2 with PHD3 knock-down MEFs compared to the shcontrol group (Figure 4D). ACC2 is hydroxylated by PHD3 (German et al., 2016) and the hydroxylation of ACC2 is essential for decreasing FAO in conditions of nutrient abundance,

indicating that PHD3 function is critical for regulating FAO (Figure 3E and 4D). To understand constitutive phosphorylation mutant on ACC2 affect FAO, we tested FAO analysis with ACC2 WT or S222E ACC2 with PHD3 overexpressing MEFs (Figure 4E). Consistent with our previous findings, the ACC2 S222E mutant, displayed higher FAO relative to ACC2 WT, which was insensitive to PHD3 expression levels (Figure 4E).

Thus, we examined the effect of PHD3 on acyl-carnitine and metabolite profiles (Figure S4C-E). Strikingly, loss of either PHD3 or AMPK in MEFs appeared to have opposing effects on global metabolite pools. These heat map data demonstrated that PHD3 KD MEFs possessed elevated acyl-carnitines, while AMPK KO MEFs showed reduced acyl-carnitines (Figure S4C). PHD3 activates ACC2 by hydroxylation (red) (German et al., 2016) and represses fat catabolism, and AMPK (blue) has a reciprocal function and activates FAO by inhibiting ACC2 (Figure 4F). Therefore, increased FAO leads to higher levels of long chain acyl-carnitines. Interestingly, AMPK-deficient MEFs showed increased levels of short chain acyl-carnitines and decreased levels of long chain acyl-carnitines, consistent with decreased FAO (Figure 4F). Opposingly, PHD3 loss increased levels of long chain acyl-carnitines and decreased levels of short chain acyl-carnitines, consistent with increased FAO (Figure 4F). Thus, AMPK loss and PHD3 loss regulate cellular FAO levels in opposing directions. Of note, the level of ACC2 or mitochondrial mass was unchanged by PHD3 loss (Figure S4F-J). Since glucose and fatty acids are both converted to acetyl-CoA, activated fat oxidation suppresses glycolysis (De Leiris et al., 1975; Randle et al., 1963; Jenkins et al., 2011). To examine whether PHD3 regulates glucose oxidation in addition to fat oxidation, we measured the basal oxygen consumption rate (OCR) resulting from glucose or fat oxidation WT or PHD3 knockdown MEFs using a Seahorse flux analyzer (Figure S4K-L). Basal glucose-driven respiration was unchanged in shPHD3 MEFs under high or low nutrient conditions compared to WT cells (Figure S4L). By contrast, loss of PHD3 increased basal fat oxidation-driven respiratory activity, consistent with increased FAO (Figure S4K). Hence, our data collectively confirm that PHD3 is an important regulator of fat metabolism.

To illuminate the metabolic adaptations driven by PHD3 *in vivo*, we analyzed the levels of long chain acyl-carnitines in WT or PHD3 KO mice quadriceps using LC-MS/MS (Figure 4G). C12, C14, C16 and C18 acyl-carnitine levels were decreased in WT quadriceps under fasted

conditions in PHD3 KO mice compared to WT mice (Figure 4H). In quadriceps we observed long chain acyl-carnitines were lower in WT mice under fasted conditions compared to fed WT mice (Figure 4H). These long chain acyl-carnitines were even lower in PHD3 KO relative to WT mice and remained low under fed or fasted conditions. Our findings were corroborated using using matrix-assisted laser desorption/ionization mass spectrometry imaging (MALDI-MSI) to assess spatial resolution of metabolite profiles *in vivo* (Figure 4J). Consistent with LC-MS/MS data, acyl-carnitines (C14 acyl-carnitine, C16 acyl-carnitine, and C18 acyl-carnitine) levels were lower in the quadriceps of PHD3 KO mice under fed conditions compared to those in WT mice in fed conditions, whereas there was no further difference in fasted PHD3 KO mice (Figure 4J-K, S5M-N). Heme levels were used for reference, which were not changed in PHD3 KO tissue (Figure 4J, S5O). Interestingly, we observed that while low glucose conditions in cells increased acyl-carnitine levels, fasting in mice decreased C14, C16 and C18 acyl-carnitines. We reasoned that these fuels might have a higher oxidization rate during fasting *in vivo*, which would prevent acyl-carnitines from accumulating. Thus, we additionally measured the rate of ^{14}C-palmitate oxidation (Figure 4L) on quadriceps slices isolated from WT and PHD3 KO mice. Indeed, palmitate oxidation increased in PHD3 KO mice quadriceps compared to WT (Figure 4L). We challenged mice with a fasting challenge and observed that FAO was increased compared to fed condition (Figure 4L). These alterations appeared in the absence of global changes in free fatty acids (FFA), triglycerides (TG), glucose, body weight or lean body mass (Figure 5A-F). Therefore, loss of PHD3 increases FAO in cells and in mouse quadriceps.

Loss of PHD3 increases exercise capacity

Since PHD3 loss activates FAO *in vitro* and *in vivo*, and ACC2 and PHD3 are highly expressed in oxidative tissues (Figure 2A). We sought to identify physiological conditions where PHD3 function may be important. In an unbiased analysis using a publicly available human skeletal muscle dataset with 242 samples (GSE3307) (Bakay et al., 2006; Dadgar et al., 2014), PHD3 expression negatively correlated with mitochondrial and FAO associated genes (Figure S5A). Next, to gain insight into the role of PHD3 in muscle physiology, we analyzed expression

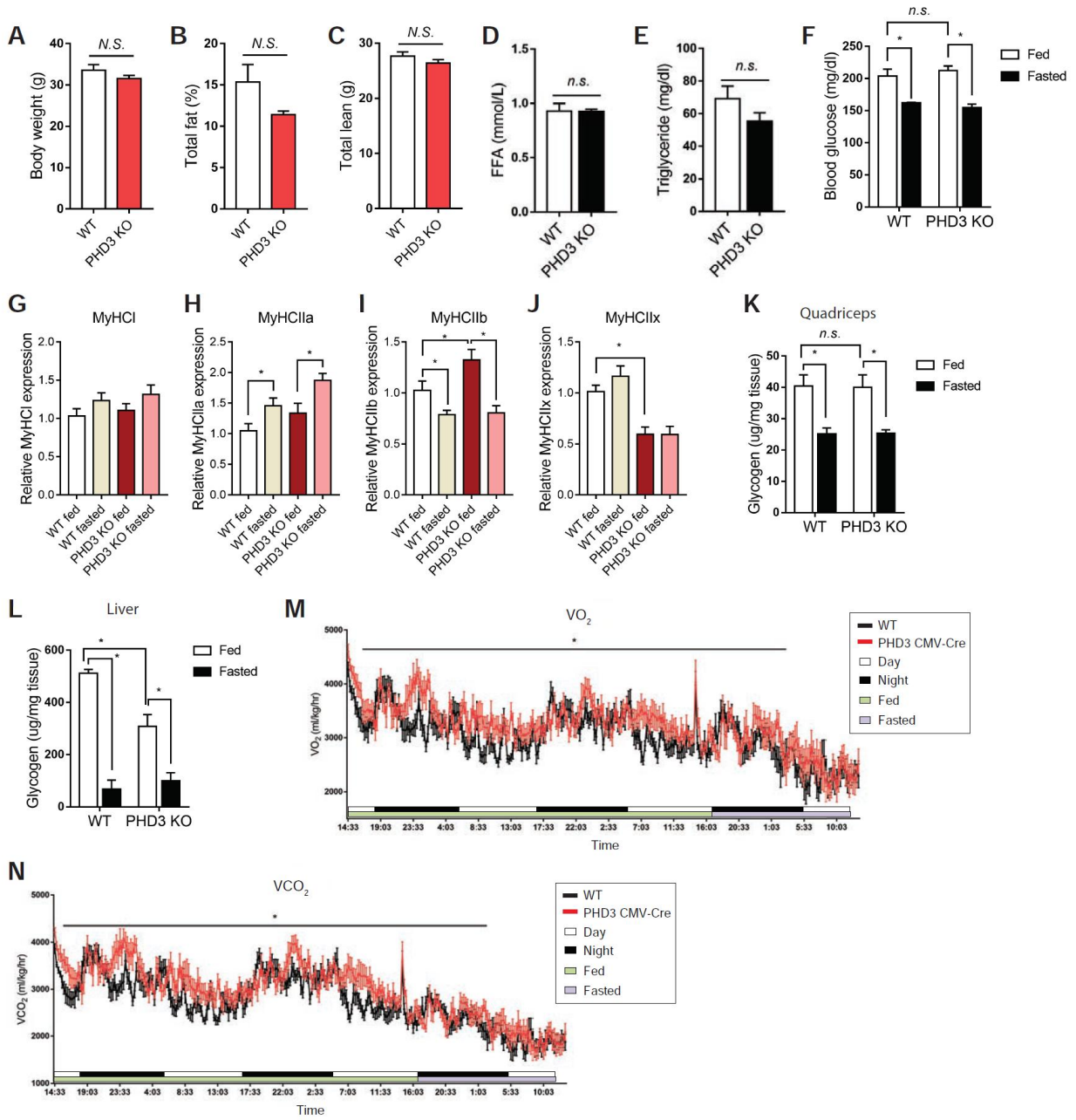

Figure 5. Characterization of PHD3 KO mice.
Metabolic parameters in 20 weeks of WT or PHD3 KO mice using DEXA imaging analysis (n = 9 mice per group). Body weight (A), total fat (B), total lean mass (C) in WT or PHD3 KO mice (n=9). Blood FFA (D) and triglyceride (E) levels using blood chemistry (n=4). (F) Blood glucose levels in WT or PHD3 KO mice under fed or fasted condition (n=9 per group). The mRNA levels of MyHCI (G), MyHCIIa (H), MyHCIIb (I) and MyHCIIx (J) in WT or PHD3 KO mouse quadriceps under fed or fasting conditions (n = 4). Glycogen levels were measured and normalized by tissue weight of WT or PHD3 KO mice quadriceps (K) or liver (L) under fed or fasted condition (n=4). (M) Mean whole-body maximum oxygen consumption rate (VO_2) in 20 weeks of WT or PHD3 KO mice using Comprehensive Lab Animal Monitoring System (CLAMS) (n=9). Animals were fed ad libitum for 48 hours and fasted for 16 hours. Data represented means ± SEM. *P < 0.05. (N) Mean whole-body CO_2 analysis (n=9).

datasets from human skeletal muscle biopsies either obtained after endurance exercise training (GSE111551). PHD3 expression was decreased in muscle biopsy samples from a post-exercise cohort but not significantly (Figure S6B). Also, PHD3 expression was not altered in quadriceps muscle by a short endurance exercise challenge in mice (Figure S6C). These results suggest

PHD3 expression negatively correlates with fat metabolism in muscle and may be potentially relevant to muscle physiology.

Thus, we investigated parameters of skeletal muscle function and physiology. We investigated whether PHD3 KO mice displayed changes in quadriceps muscle fiber type by measuring the gene expression of Myosin heavy chain 1 (MyHCI) and Myosin heavy chain 2 (MYH2), which are type I and type II fiber markers, respectively (Figure 5G-J) (Bloemberg and Quadrilatero, 2012). Compared with control animals PHD3 KO mice displayed similar expression of MyHCI, MyHCIIa, MyHCIIb and MyHCIIx (Figure 5G-J). We also examined the gene expression of muscle differentiation markers MyoD which were increased, and myoglobin which were not changed in PHD3 KO quadriceps compared to WT tissue (Figure S5D-F). Moreover, there was no change in MYH2 and ACC2 protein level in PHD3 and WT quadriceps using immunofluorescence staining (Figure S5).

Distinct from reported mitochondrial biogenesis associated with AMPK activation (REF), PHD3 KO mouse quadriceps showed similar gene expression of TFB1M, TFB2M, PGC1α, cytochrome C, PDK4, and PPARα (Figure S5I). As glycogen serves as a major source of stored energy, we also measured quadriceps and liver glycogen levels (Figure 5K-L). The level of glycogen in quadriceps was unchanged in PHD3 KO mice compared with WT animals. In the liver, glycogen levels were reduced in fed PHD3 KO mice, but there was no significant difference between the lower glycogen levels in WT or PHD3 KO livers upon fasting. Finally, we examined whole body energy homeostasis in PHD3 KO animals by measuring the oxygen consumption (VO_2), CO_2 release (VCO_2) and respiratory exchange ratio (RER) of WT and PHD3 KO mice in fed versus fasted states (Figure 5M-N, S5J). VO_2 was increased in PHD3 KO mice during the comprehensive lab animal monitoring system (CLAMS) compared to WT (Figure 5M). Also, VCO_2 was increased in PHD3 KO mice and RER was not significantly changed in this animals compared to WT (Figure 5N and S5J). Overall, these data reveal that there were not dramatic alterations in skeletal muscle development in PHD3 KO animals whole body energy homeostasis.

During exercise, muscle cells oxidize fatty acids, in addition to carbohydrates, to support energy demand (Spriet, 2014; Mul et al., 2015). Previous studies have shown that AMPK

increases body energy expenditure though phosphorylation of ACC2 (O'Neill et al., 2014; Galic et al., 2018). Loss of ACC2 increases exercise capacity (Choi et al., 2007; Cho et al., 2010; Abu-Elheiga et al., 2003), and AMPK activators, such as AICAR, have been shown to increase exercise tolerance by up to 44%, by inducing mitochondrial gene expression and biogenesis (Narkar et al., 2008). Thus, we reasoned that PHD3 loss may be important physiologically during the challenge of exercise tolerance. Based on our biochemical, metabolic, and *in vivo* data supporting a reciprocal interaction between AMPK and PHD3, we hypothesized that PHD3 KO mice would possess increased energy expenditure and exercise capacity, and may phenocopy aspects of AMPK activation *in vivo*. To test this idea, we analyzed exercise endurance in control and PHD3 KO mice using a metabolic treadmill with a gradually increasing incline (Figure 6A, Figure S6A). Remarkably, during the exercise endurance challenge PHD3 KO mice displayed a significantly increased VO_2, particularly during the high incline period (Figure 6B); thus, loss of PHD3 function enabled animals to maintain elevated VO_2 during rigorous exercise. Consistent with elevated metabolic fitness, PHD3 KO animals generated more VCO_2 (Figure S6C). PHD3 KO mice ran for 40% longer time and >50% further distance compared with WT animals (Figure 6C-E). The maximal oxygen consumption rate (VO_{2max}) was unchanged between WT and PHD3 KO animals (Figure S6B). However, WT mice reached VO_{2max} sooner than PHD3 KO animals, consistent with the finding that PHD3 KO mice had more overall exercise endurance (Fig 6E).

Mechanistically, we tested whether ACC2 hydroxylation changed in exercised skeletal muscle. As expected, loss of PHD3 decreased ACC2 hydroxylation in quadriceps muscle (Figure 2E, Figure 6F). Strikingly, while ACC2 protein levels were unchanged, ACC2 hydroxylation was nearly undetectable in skeletal muscle isolated from mice immediately after endurance exercise. This hydroxylation was dependent upon PHD3, as PHD3 KO mice demonstrated little to no ACC2 hydroxylation in either condition. As expected, the phosphorylation of ACC2 was increased by exercise, and was equally induced with similar kinetics in skeletal muscle from PHD3 KO animals (Figure 6F). To understand the role of PHD3 dependent FAO in exercise, we measured the rate of ^{14}C-palmitate oxidation on quadriceps slices isolated from WT and PHD3 KO mice after endurance exercise. Parallel with hydroxylation of ACC2, *ex vivo* FAO was increased in WT mice quadriceps in post-exercise compared to pre-exercise (Figure 6G). Also, the quadriceps of PHD3 KO mice had higher FAO compared to WT (Figure 6G). Interestingly,

PHD3 KO mouse quadriceps showed increasing gene expression of VEGF, TFB1M, TFB2M, PGC1α, PDK4, and PPARα after endurance exercise compared to WT animals (Figure S6E).

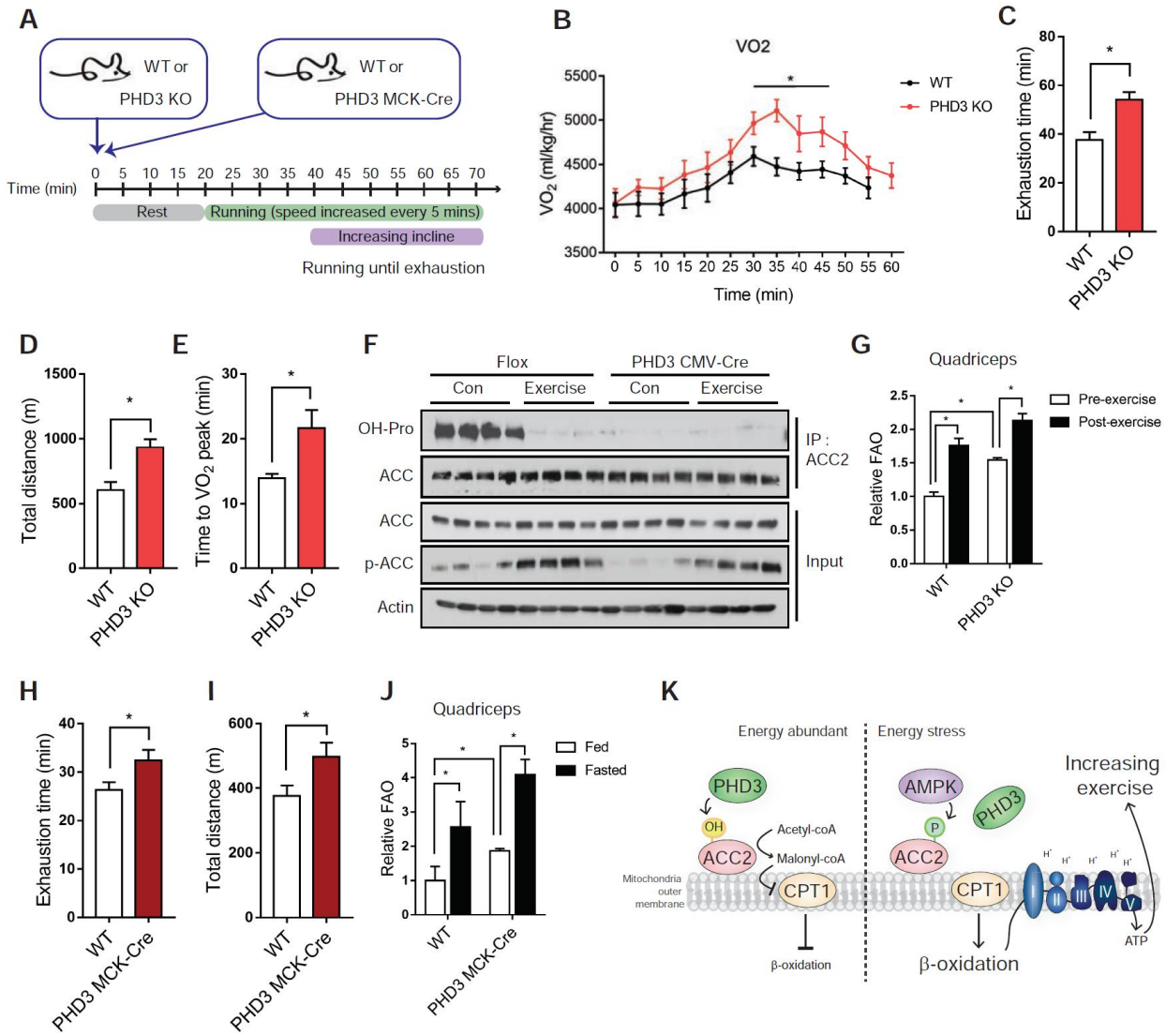

Figure 6. Loss of PHD3 increases exercise capacity.
(A) Flowchart of the endurance exercise experiments. (B) PHD3 KO mice demonstrated increased exercise tolerance compared to WT control mice after repetitive treadmill running (n = 8 mice per group). Mean whole-body maximum oxygen consumption rate of both genotypes was calculated from the individual performances during treadmill running. The individual exhaustion time (C), total running distance (D) and time to maximum oxygen consumption rate (E). Data represent means ± SEM. *P < 0.05. (F) Immunoprecipitation and western blotting analysis of ACC2 hydroxylation and phosphorylation in WT or PHD3 KO mouse quadriceps under control or exercise conditions (n = 4). (G) Palmitate oxidation in WT or PHD3 KO mice quadriceps under pre- or post-exercise conditions using ^{14}C-labeled palmitate and CO_2 capture FAO analysis (n=3). The individual exhaustion time (H), total distance for running (I) during treadmill running with WTfl/fl and PHD3 muscle specific knock-out mice (PHD3 MCK-Cre). (J) Palmitate oxidation in control or PHD3 MCK-Cre mice quadriceps under fed or fasted condition using ^{14}C-labeled palmitate and CO_2 capture FAO analysis (n=4). (K) Schematic that loss of PHD3 induces exercise capacity. PHD3 hydroxylates ACC2 to represses FAO and AMPK induces FAO by inhibiting PHD3 binding into ACC2.

To test whether PHD3 loss of function in skeletal muscle was sufficient to increase exercise capacity, we generated MCK-Cre driven PHD3 knockout mice (PHD3 MCK-Cre), to delete PHD3 specifically in muscles. Indeed, PHD3 levels were decreased in quadriceps of PHD3 MCK-Cre mice compared to WT (Figure S6F) muscle, but were unchanged in the liver.

When given an endurance exercise challenge, PHD3 MCK-Cre mice remained on the treadmill for 23% longer time and ran 32% further distance compared with WT animals (Figure 6H-I). Consistent with our findings in cells and in tissues from PHD3 whole body KO animals, ACC2 hydroxylation was nearly undetectable in PHD3 MCK-Cre quadriceps muscle (Figure S6G). Next, we measured FAO from *ex vivo* slices of WT or PHD3 MCK-Cre quadriceps (Figure 6J). In both WT and PHD3 MCK-Cre quadriceps, FAO was increased after a 16-hour fast compared to fed conditions. However, PHD3 MCK-Cre quadriceps displayed elevated FAO compared with WT quadriceps (Figure 6J). In sum, these results demonstrate that PHD3 loss specifically in skeletal muscle is sufficient for increased exercise capacity.

DISCUSSION

Here, we elucidate a fundamental mechanism that mediates the dynamic regulation of fatty acid metabolism in response to bioenergetic stress. AMPK and PHD3 coordinate their catalytic activities sequentially on ACC2 to alter fatty acid metabolism in conditions of stress (Figure 3K). Mechanistically, during energetic stress, AMPK phosphorylation of ACC2 impedes the binding interaction between ACC2 and PHD3, consequently inhibiting ACC2 hydroxylation (Figure 6K). Importantly, hydroxylation of ACC2 does not affect AMPK binding to or phosphorylation of ACC2. Thus, PHD3 appears to counterbalance AMPK signaling to regulate fatty acid metabolism in response to changing nutrient availability through altered binding affinity to ACC2. During physiological energy challenges, such as fasting or exercise endurance, PHD3 KO mice display greater oxidative metabolism and increased exercise capacity. Therefore, PHD3 and AMPK act coordinately as sensors to regulate energy homeostasis, in part, via convergent regulation of ACC2.

How do PTMs control ACC2 activity? First, oligomerization is a key regulator of ACC2 function; the monomeric form is inactive while the dimerized and multi-oligomerized form is active. Phosphorylation of S222 shifts ACC2 into the inactive monomeric form, demonstrating that ACC2 PTMs can affect oligomerization state. Interestingly, recent studies have shown that oligomerization of ACC2 is mediated by the BC domain, which contains the P450 residue that is hydroxylated by PHD3 (Wei and Tong, 2014; German et al., 2016). S222 and P450 are not adjacent in the amino acid sequence; yet, when the human ACC2 biotin carboxylase domain

(PDB: 3JRW) (Cho et al., 2010) was superimposed with the cryo-electron microscopy ACC structure from yeast (PDB: 5CSL) (Wei and Tong, 2015), it became apparent that the distance between these residues may be only ~ 50 Å (Figure 3A). The potential proximity of S222 and P450 lead us to postulate that ACC2 phosphorylation may either sterically or allosterically hinder PHD3 binding and subsequent hydroxylation of ACC2. Since PHD3 hydroxylation enhances ACC2 binding to ATP and promotes activity, it will be interesting for future studies to probe whether PHD3-mediated hydroxylation likewise promotes ACC2 oligomerization.

ACC2 phosphorylation by AMPK is increased during energy stresses, such as fasting, exercise, or high fat diet challenge (Cho et al., 2010; O'Neill et al., 2014; Gwinn et al., 2008; Vasquez et al., 2008; Mihaylova and Shaw, 2011). Interestingly, PHD3 loss mimics the phenotypes associated with AMPK activation. For example, in this study we demonstrate that PHD3 loss enables mice to maintain high VO_2 during an exercise challenge and run >50% further on an incline (Figure 6B and 6D). The muscle and liver glycogen levels, blood glucose levels and RER were similar in PHD3 KO and WT mice (Figure 5F, 5K-L). Since PHD3 KO mice had higher VO2 peak (Figure 6B and 6E), we concluded that PHD3 KO mice had higher exercise capacity. Of note, increased exercise capacity can be observed in mice with muscle-specific deletion of PHD3, demonstrating a tissue autonomous role for PHD3 in skeletal muscle during exercise challenge. These results are consistent with elevated FAO observed in PHD3 KO mouse muscle, and constitutive phosphorylation of ACC2 in this system (Figure 6F-G). The mechanism of changing work performance is beyond the scope of our results, which is focused on the coordination of PHD3 and AMPK PTMs on ACC2. We demonstrate that physiological activation of AMPK is sufficient to repress PHD3-mediated ACC2 hydroxylation. Interestingly, our data shows that ACC2 hydroxylation in heart tissue is profoundly responsive to fed/fasting status (Figure 2C). Therefore, these changes in exercise performance also might be related to cardiac function.

Our results reveal that PHD3 and AMPK reciprocally regulate fat metabolism and exercise capacity via their coordinate regulation of ACC2. During energy stress, AMPK-mediated phosphorylation inhibits PHD3 interaction with and hydroxylation of ACC2. Upon energy replete conditions, AMPK is inactive, ACC is not phosphorylated, and PHD3 is able to hydroxylate ACC2 (Figure 6K). Collectively, these data suggest that PHD3 loss or inhibition

could be a new strategy for treatment of a wide range of metabolic diseases, and that modulation of PHD3 may improve energy homeostasis and skeletal muscle performance during a wide range of physiological stresses.

STAR METHODS

Detailed methods are provided in this paper and include the following:

- KEY RESOURCES TABLE
- CONTACT FOR REAGENT AND RESOURCE SHARING
- EXPERIMENTAL MODEL AND SUBJECT DETAILS
    - Cell Lines
    - Mice
- METHOD DETAILS
    - Preparation of plasmids, siRNAs and transfection
    - Quantitative RT-PCR analysis
    - Immunoprecipitation, western blotting and antibodies
    - *In vitro* protein binding assay
    - Immunofluorescence
    - Molecular modeling
    - Fatty acid oxidation measurements
    - MT-DNA quantification
    - Mitochondrial mass quantification
    - Respiration
    - Metabolite profiling and mass spectrometry
    - GeLC-MS/MS
    - MALDI MSI
    - Exercise performance studies
    - Histological procedures
    - Bioinformatics analysis
- QUANTIFICATION AND STATISTICAL ANALYSIS

SUPPLEMENT INFORMATION

Supplement Information includes seven figures and one table.

ACKNOWLEDGEMENTS

We thank all members of the Haigis lab for thoughtful discussion on this manuscript. H.Y. is funded by the American Diabetes Association Fellowship (1-17-PDF-109) and M.C.H is funded by NIH grant R01CA213062, the Ludwig Center at Harvard University, and Glenn Foundation for Medical Research. J.A. is funded by the Ecole Polytechnique Fédérale de Lausanne and the Fondation Suisse de Recherche sur les Maladies Musculaires. A.C., A.D., L.J.G is funded by the Joslin Core grant (NIH P30DK036836). E.C.R. is in receipt of an NIH R25 (R25 CA-89017) Fellowship in partnership with the Ferenc Jolesz National Center for Image Guided Therapy at BWH (P41 EB015898). H.Y. and M.C.H are co-inventors on the patent case number-HU 7395 submitted by Harvard Medical School that Dynamic regulation of fat metabolism by Acetyl CoA Carboxylase. Microscopy experiments were performed at the Nikon Imaging Center at Harvard Medical School. Mouse exercise experiments were performed at Joslin Diabetes Center. pHAGE-CMV-Flag-HA-puromycin vector was obtained from Wade Harper's lab at Harvard Medical School. cDNA and entry vectors were obtained from the Dana Farber/ Harvard Cancer Center Resource Core.

AUTHOR CONTRIBUTIONS

H.Y. and M.C.H. designed experiments, wrote the paper, and analyzed data. H.Y, J.B.S., P.J.A., and S.P.G performed and analyzed mass spectrometry experiments. H.Y., E.Z., and S.J.W. conducted *in vivo* mouse experiments. E.C.R performed mass spectrometry imaging and data analysis, N.Y.R.A. contributed analytical tools. H.Y., A.D., A.C., and L.J.G performed mouse exercise experiment in Joslin Diabetes Center. H.Y., E.Z., S.J.W, and N.J.G performed experiments on gene expression, protein levels and post-translational modification. D.G., and R.J.S provided tissue samples for AMPK KO mice. H.Y. H.L., and J.A. performed bioinformatics analysis. H.Y. performed structure modeling.

REFERENCES

Abu-Elheiga, L., Oh, W., Kordari, P., and Wakil, S.J. (2003). Acetyl-CoA carboxylase 2 mutant mice are protected against obesity and diabetes induced by high-fat/high-carbohydrate diets. Proc. Natl. Acad. Sci. USA *100*, 10207-10212.

Bakay, M., Wang, Z., Melcon, G., Schiltz, L., Xuan, J., Zhao, P., Sartorelli, V., Seo, J., Pegoraro, E., Angelini, C., et al. (2006). Nuclear envelope dystrophies show a transcriptional fingerprint suggesting disruption of Rb-MyoD pathways in muscle regeneration. Brain *129*, 996-1013.

Berberich, M.J., Paulo, J.A., and Everley, R.A. (2018). MS3-IDQ: Utilizing MS3 Spectra beyond Quantification Yields Increased Coverage of the Phosphoproteome in Isobaric Tag Experiments. J. Proteome Res. *17*, 1741-1747.

Bloemberg, D., and Quadrilatero, J. (2012). Rapid determination of myosin heavy chain expression in rat, mouse, and human skeletal muscle using multicolor immunofluorescence analysis. PLoS One. *7*, e35273.

Carling, D., Clarke, P.R., Zammit, V.A., and Hardie, D.G. (1989). Purification and characterization of the AMP-activated protein kinase. Copurification of acetyl-CoA carboxylase kinase and 3-hydroxy-3-methylglutaryl-CoA reductase kinase activities. Eur. J. Biochem. *186*, 129-136.

Chen, Y., Zhang, H.S., Fong, G.H., Xi, Q.L., Wu, G.H., Bai, C.G., Ling, Z.Q., Fan, L., Xu, Y.M., Qin, Y.Q., et al. (2015). PHD3 Stabilizes the Tight Junction Protein Occludin and Protects Intestinal Epithelial Barrier Function. J. Biol. Chem. *290*, 20580-20589.

Cho, Y.S., Lee, J.I., Shin, D., Kim, H.T., Jung, H.Y., Lee, T.G., Kang, L.W., Ahn, Y.J., Cho, H.S., and Heo, Y.S. (2010). Molecular mechanism for the regulation of human ACC2 through phosphorylation by AMPK. Biochem. Biophys. Res. Commun. *391*, 187-192.

Choi, C.S., Savage, D.B., Abu-Elheiga, L., Liu, Z.X., Kim, S., Kulkarni, A., Distefano, A., Hwang, Y.J., Reznick, R.M., Codella, R., et al. (2007). Continuous fat oxidation in acetyl-CoA carboxylase 2 knockout mice increases total energy expenditure, reduces fat mass, and improves insulin sensitivity. Proc. Natl. Acad. Sci. USA *104*, 16480-16485.

Chouchani, E.T., Kazak, L., Jedrychowski, M.P., Lu, G.Z., Erickson, B.K., Szpyt, J., Pierce, K.A., Laznik-Bogoslavski, D., Vetrivelan, R., Clish, C.B., et al. (2016). Mitochondrial ROS regulate thermogenic energy expenditure and sulfenylation of UCP1. Nature *532*, 112-116.

Dadgar, S., Wang, Z., Johnston, H., Kesari, A., Nagaraju, K., Chen, Y.W., Hill, D.A., Partridge, T.A., Giri, M., Freishtat, R.J., et al. (2014). Asynchronous remodeling is a driver of failed regeneration in Duchenne muscular dystrophy. J. Cell Biol. *207*, 139-158.

De Leiris, J., Opie, L.H., and Lubbe, W.F. (1975). Effects of free fatty acid and enzyme release in experimental glucose on myocardial infarction. Nature *253*, 746-747.

Efeyan, A., Comb, W.C., and Sabatini, D.M. (2015). Nutrient-sensing mechanisms and pathways. Nature *517*, 302-310.

Errichiello, E., Balsamo, A., Cerni, M., and Venesio, T. (2015). Mitochondrial variants in MT-CO2 and D-loop instability are involved in MUTYH-associated polyposis. J. Mol. Med. (Berl). *93*, 1271-1281.

Galgani, J., and Ravussin, E. (2008). Energy metabolism, fuel selection and body weight regulation. Int. J. Obes. (Lond). *Suppl 7*, S109-119.

Galic, S., Loh, K., Murray-Segal, L., Steinberg, G.R., Andrews, Z.B., and Kemp, B.E. (2018). AMPK signaling to acetyl-CoA carboxylase is required for fasting- and cold-induced appetite but not thermogenesis. Elife *13*, pii: e32656.

German, N.J., Yoon, H., Yusuf, R.Z., Murphy, J.P., Finley, L.W., Laurent, G., Haas, W., Satterstrom, F.K., Guarnerio, J., Zaganjor, E., et al. (2016). PHD3 Loss in Cancer Enables Metabolic Reliance on Fatty Acid Oxidation via Deactivation of ACC2. Mol. Cell *63*, 1006-1020.

Gordon, P.M., Liu, D., Sartor, M.A., IglayReger, H.B., Pistilli, E.E., Gutmann, L., Nader, G.A., and Hoffman, E.P. (1985). Resistance exercise training influences skeletal muscle immune activation: a microarray analysis. J. Appl. Physiol. *112*, 443-453.

Gowans, G.J., and Hardie, D.G. (2014). AMPK: a cellular energy sensor primarily regulated by AMP. Biochem. Soc. Trans. *42*, 71-75.

Greenberg, S.A., Bradshaw, E.M., Pinkus, J.L., Pinkus, G.S., Burleson, T., Due, B., Bregoli, L., O'Connor, K.C., and Amato, A.A. (2005). Plasma cells in muscle in inclusion body myositis and polymyositis. Neurology *65*, 1782-1787.

Grunt, T.W. (2018). Interacting Cancer Machineries: Cell Signaling, Lipid Metabolism, and Epigenetics. Trends. Endocrinol. Metab. *29*, 86-98.

Gwinn, D.M., Shackelford, D.B., Egan, D.F., Mihaylova, M.M., Mery, A., Vasquez, D.S., Turk, B.E., and Shaw, R.J. (2008). AMPK phosphorylation of raptor mediates a metabolic checkpoint. Mol. Cell *30*, 214-226.

Hardie, D.G., Ross, F.A., and Hawley, S.A. (2012). AMPK: a nutrient and energy sensor that maintains energy homeostasis. Nat. Rev. Mol. Cell Biol. *13*, 251-262.

Herzig, S., and Shaw, R.J. (2018). AMPK: guardian of metabolism and mitochondrial homeostasis. Nat. Rev. Mol. Cell Biol. *19*, 121-135.

Hunter, R.W., Treebak, J.T., Wojtaszewski, J.F., and Sakamoto, K. (2011). Molecular mechanism by which AMP-activated protein kinase activation promotes glycogen accumulation in muscle. Diabetes *60*, 766-774.

Inoki, K., Zhu, T., and Guan, K.L. (2003). TSC2 mediates cellular energy response to control cell growth and survival. Cell *26*, 577-590.

Jacobs, R.A., Díaz, V., Meinild, A.K., Gassmann, M., and Lundby, C. (2013). The C57Bl/6 mouse serves as a suitable model of human skeletal muscle mitochondrial function. Exp. Physiol. *98*, 908-921.

Jenkins, C.M., Yang, J., Sims, H.F., and Gross, R.W. (2011). Reversible high affinity inhibition of phosphofructokinase-1 by acyl-CoA: a mechanism integrating glycolytic flux with lipid metabolism. J. Biol. Chem. *286*, 11937-11950.

Laderoute, K.R., Amin, K., Calaoagan, J.M., Knapp, M., Le, T., Orduna, J., Foretz, M., and Viollet, B. (2006). 5'-AMP-activated protein kinase (AMPK) is induced by low-oxygen and glucose deprivation conditions found in solid-tumor microenvironments. Mol. Cell Biol. *26*, 5336-5347.

Lee, S., Nakamura, E., Yang, H., Wei, W., Linggi, M.S., Sajan, M.P., Farese, R.V., Freeman, R.S., Carter, B.D., Kaelin, W.G. Jr. et al. (2005). Neuronal apoptosis linked to EglN3 prolyl hydroxylase and familial pheochromocytoma genes: developmental culling and cancer. Cancer Cell *8*, 155-167.

Lee, J., Choi, J., Scafidi, S., and Wolfgang, M.J. (2016). Hepatic Fatty Acid Oxidation Restrains Systemic Catabolism during Starvation. Cell Rep. *16*, 201-212.

Liu, X., Ide, J.L., Norton, I., Marchionni, M.A., Ebling, M.C., Wang, L.Y., Davis, E., Sauvageot, C.M., Kesari, S., Kellersberger, K.A., et al. (2013). Molecular imaging of drug transit through the blood-brain barrier with MALDI mass spectrometry imaging. Sci. Rep. *3*, 2859.

Manning, B.D., Toker, A. (2017). AKT/PKB Signaling: Navigating the Network. Cell *169*, 381-405.

McCoin, C.S., Knotts, T.A., and Adams, S.H. (2015). Acylcarnitines--old actors auditioning for new roles in metabolic physiology. Nat. Rev. Endocrinol. *11*, 617-625.

Mihaylova, M.M., and Shaw, R.J. (2011). The AMPK signalling pathway coordinates cell growth, autophagy and metabolism. Nat. Cell Biol. *13*, 1016-1023.

Millay, D.P., O'Rourke, J.R., Sutherland, L.B., Bezprozvannaya, S., Shelton, J.M., Bassel-Duby, R., Olson, E.N. (2013). Myomaker is a membrane activator of myoblast fusion and muscle formation. Nature *499*, 301-330.

Mul, J.D., Stanford, K.I., Hirshman, M.F., and Goodyear, L.J. (2015). Exercise and Regulation of Carbohydrate Metabolism. Prog. Mol. Biol. Transl. Sci. *135*, 17-37.

Narkar, V.A., Downes, M., Yu, R.T., Embler, E., Wang, Y.X., Banayo, E., Mihaylova, M.M., Nelson, M.C., Zou, Y., Juguilon, H., et al. (2008). AMPK and PPARdelta agonists are exercise mimetics. Cell *134*, 405-415.

Navarrete-Perea, J., Yu, Q., Gygi, S.P., and Paulo, J.A. (2018). Streamlined Tandem Mass Tag (SL-TMT) Protocol: An Efficient Strategy for Quantitative (Phospho)proteome Profiling Using Tandem Mass Tag-Synchronous Precursor Selection-MS3. J. Proteome Res. *17*, 2226-2236.

O'Neill, H.M., Maarbjerg, S.J., Crane, J.D., Jeppesen, J., Jørgensen, S.B., Schertzer, J.D., Shyroka, O., Kiens, B., van Denderen, B.J., Tarnopolsky, M.A., et al. (2011). AMP-activated protein kinase (AMPK) beta1beta2 muscle null mice reveal an essential role for AMPK in maintaining mitochondrial content and glucose uptake during exercise. Proc. Natl. Acad. Sci. USA *108*, 16092-16097.

O'Neill, H.M., Lally, J.S., Galic, S., Thomas, M., Azizi, P.D., Fullerton, M.D., Smith, B.K., Pulinilkunnil, T., Chen, Z., Samaan, M.C., et al. (2014). AMPK phosphorylation of ACC2 is

required for skeletal muscle fatty acid oxidation and insulin sensitivity in mice. Diabetologia *57*,1693-1702.

Palm, W., and Thompson, C.B. (2017). Nutrient acquisition strategies of mammalian cells. Nature *546*, 234-242.

Paulo, J.A. (2016). Sample preparation for proteomic analysis using a GeLC-MS/MS strategy. J. Biol. Methods *3*, pii: e45.

Randle, P.J., Garland, P.B., Hales, C.N., and Newsholeme, E.A. (1963). The glucose fatty-acid cycle. Its role in insulin sensitivity and the metabolic disturbances of diabetes mellitus. Lancet *1*, 785-789.

Raue, U., Trappe, T.A., Estrem, S.T., Qian, H.R., Helvering, L.M., Smith, R.C., and Trappe, S. (1985). Transcriptome signature of resistance exercise adaptations: mixed muscle and fiber type specific profiles in young and old adults. J. Appl. Physiol. *112*, 1625-1636.

Ruzankina, Y., Pinzon-Guzman, C., Asare, A., Ong, T., Pontano, L., Cotsarelis, G., Zediak, V.P., Velez, M., Bhandoola, A., and Brown, E.J. (2007). Deletion of the developmentally essential gene ATR in adult mice leads to age-related phenotypes and stem cell loss. Cell Stem Cell *1*, 113-126.

Salt, I.P., Johnson, G., Ashcroft, S.J., and Hardie, D.G. (1998). AMP-activated protein kinase is activated by low glucose in cell lines derived from pancreatic beta cells, and may regulate insulin release. Biochem. J. *335*, 533-539.

Spinelli, J.B., and Haigis, M.C. (2018). The multifaceted contributions of mitochondria to cellular metabolism. Nat. Cell Biol. *20*, 745-754.

Spriet, L.L. (2014). New insights into the interaction of carbohydrate and fat metabolism during exercise. Sports Med. *Suppl 1*, S87-96.

Takeda, K., Ho, V.C., Takeda, H., Duan, L.J., Nagy, A., and Fong, G.H. (2006). Placental but not heart defects are associated with elevated hypoxia-inducible factor alpha levels in mice lacking prolyl hydroxylase domain protein 2. Mol. Cell Biol. *26*, 8336-8346.

Tennant, D.A., and Gottlieb, E. (2010). HIF prolyl hydroxylase-3 mediates alpha-ketoglutarate-induced apoptosis and tumor suppression. J. Mol. Med. (Berl). *88*, 839-849.

Tong, L., and Harwood, H.J. Jr. (2006). Acetyl-coenzyme A carboxylases: versatile targets for drug discovery. J. Cell Biochem. *99*, 1476-1488.

Tran, T.H., Hsiao, Y.S., Jo, J., Chou, C.Y., Dietrich, L.E., Walz, T., and Tong, L. (2015). Structure and function of a single-chain, multi-domain long-chain acyl-CoA carboxylase. Nature *518*, 120-124.

Wei, J., and Tong, L. (2015). Crystal structure of the 500-kDa yeast acetyl-CoA carboxylase holoenzyme dimer. Nature *526*, 723-727.

Woods, S.C., and Ramsay, D.S. (2011). Food intake, metabolism and homeostasis. Physiol. Behav. *104*, 4-7.

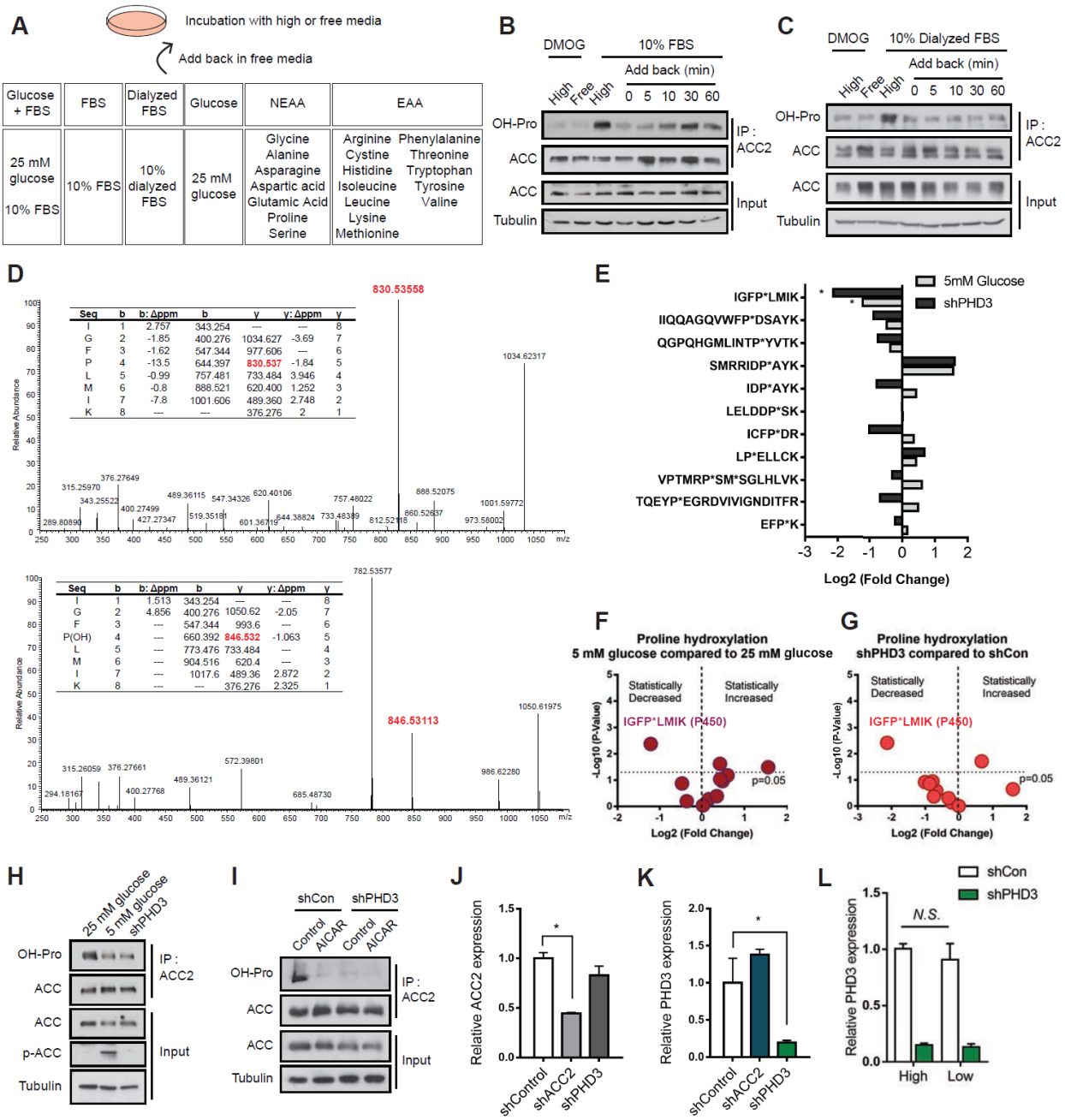

Figure S1.The hydroxylation of proline 450 residue is most changed by nutrient-depleted conditions as well as PHD3 depletion compared to high nutrient conditions. (A) Schematic depicting of the different fuels to which cells in culture are exposed. After addback, cells were used for ACC2 hydroxylation assay. Hydroxylation was assessed after 12 h incubation in high or nutrient-free media, and then 0 to 60 min after 10% FBS (B), and 10% dialyzed FBS (C) re-addition. Hydroxylation was detected by western blotting. (D) Representative mass spectra identifying the hydroxylated and non-hydroxylated versions of residue P450 in pulled down ACC2 protein. "b" fragments contain the N-terminal amino acid and are labeled from the N to C terminus. "y" fragments contain the C-terminal amino acid and are labeled from the C to N terminus. (E) Relative abundance of hydroxylation of proline residues on ACC2 in 5 mM glucose media incubated (dark grey) or depleted of PHD3 (light grey) compared to control cells. For all comparisons two-tailed t test was used. $P < 0.05$. Volcano plots demonstrating that 5 mM glucose media (F) or PHD3-depleted MEFs (G) incubated MEFs have statistically significant proline hydroxylation changes compared to control cells. The proline 450 residue, the sequence of which is IGFP(OH)LMIK, is most significantly changed. (H) Immunoprecipitation and western blotting analysis of ACC2 hydroxylation and phosphorylation in indicated condition. shControl or shPHD3 293T cells were transfected with ACC2, and incubated with 25 mM glucose media or 5 mM glucose media for 4 h. ACC2 proteins were pulled down using antibody against ACC2 and immunoblotted using the indicated antibodies. (I) Immunoblots of ACC2 hydroxylation from MEFs expressing either control shRNA or PHD3 shRNA with or without AICAR. (J) Relative ACC2 expression using mouse β-actin as a reference gene in MEFs expressing shRNA against ACC2, PHD3 or shRNA control (n = 4). (K) Relative PHD3 expression using mouse β-actin as a reference gene in MEFs expressing shRNA against ACC2, PHD3 or shRNA control (n = 4). (L) PHD3 expression using mouse b-actin as a reference gene in MEFs under high or low nutrient conditions.

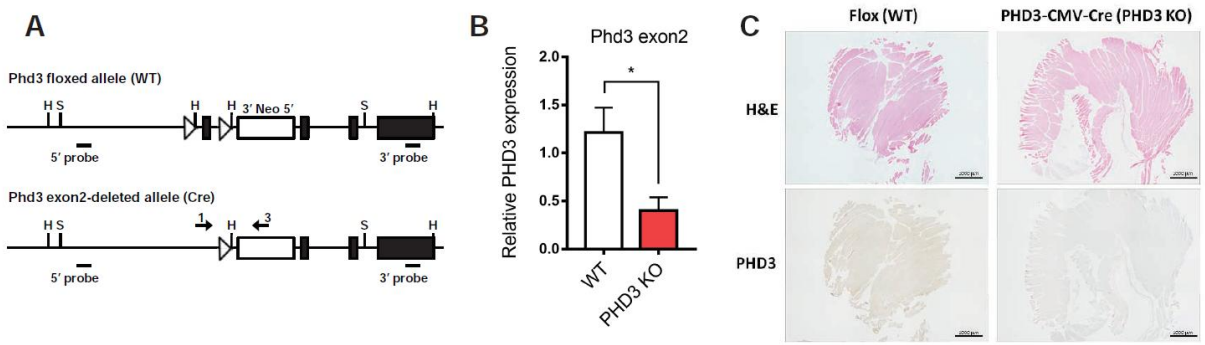

Figure S2 Estabishment of PHD3 KO mice.
(A) Gene targeting strategy for Phd3. In targeted Phd3 locus, exon 2 is flanked by two loxP sites. Exon 2 is deleted by Cre-mediated recombination. S, Sca I; H, Hind III; Neo, neomycin cassette; hatched square, Frt site (flanking the Neo cassette); open triangle, loxP site; arrows 1, 2 and 3. (B) qPCR analyses to confirm the lack of WT mRNA transcripts in PHD3 KO mouse RNA samples. (C) H&E and immunohistochemistry staining of PHD3 in WT or PHD3 KO mice muscles. Scale is 100 μm.

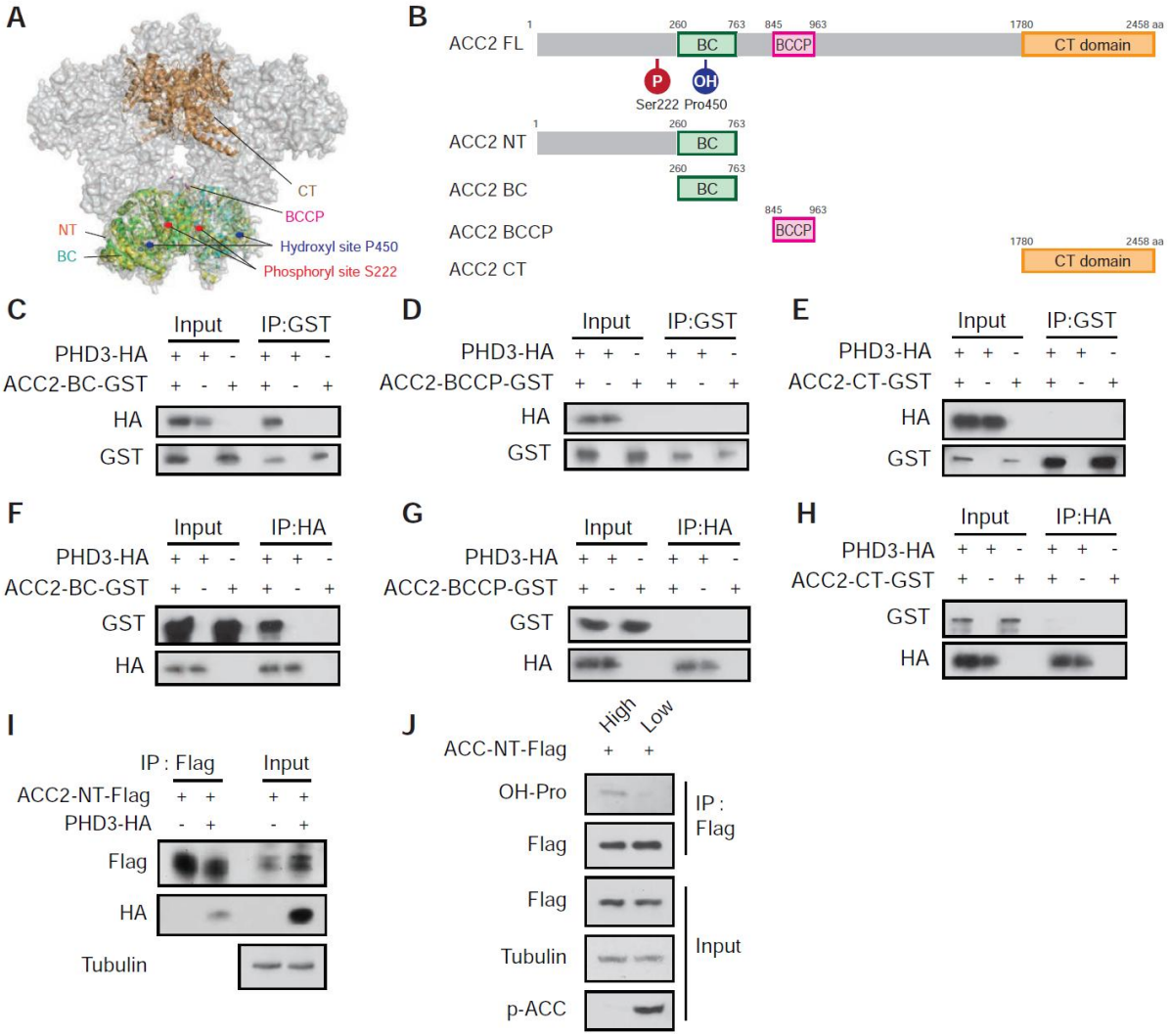

Figure S3. PHD3 binds the BC domain of ACC2.
(A) P450 (hydroxylation site, blue) is located in the ACC2 BC domain (green and cyan). S222 (phosphorylation site, red) is located inside of the ACC holoenzyme dimer structure. This model was generated by superposition of human ACC2 biotin carboxylase domain (PDB: 3JRW) with the entire yeast ACC (PDB: 5CSL). (B) Schematic figure of the domains of ACC2 protein. Posttranslational modifications by AMPK (phosphorylation, red) and PHD3 (hydroxylation, blue) are highlighted. BC, biotin carboxylase domain; BCCP, biotin carboxyl carrier protein domain; CT, carboxyltransferase domain; N-terminus domain contains ATP grasp domain. (C) Immunoprecipitation and western blotting analysis of PHD3 interaction with the BC domain of ACC2. Each proteins were extracted from E. coli. ACC2 BC domain with GST-tag and PHD3-HA was pulled down using HA-beads for an in vitro binding assay, and the precipitates were immunoblotted. (D) In vitro binding assay of PHD3 interaction with the BCCP domain using HA-beads. (E) In vitro binding assay of PHD3 interaction with the CT domain using HA-beads. (F) Immunoprecipitation and western blotting analysis of PHD3 interaction with the BC domain of ACC2. In vitro binding assay of PHD3 interaction with the BCCP domain (G) or CT domain (H). (I) ACC2 N-terminus domain interacts with PHD3. ACC2 NT-Flag and/or PHD3-HA were transfected into HEK293T cells. Proteins in cell lysates were precipitated by anti-Flag antibody and the precipitates were immunoblotted using the indicated antibodies. (J) ACC2 NT-Flag was transfected into HEK293T cells. Cells were incubated under high or low nutrient media for 8 hr. Proteins in cell lysates were precipitated by anti-Flag antibody and the precipitates were immunoblotted using hydroxyl proline antibodies.

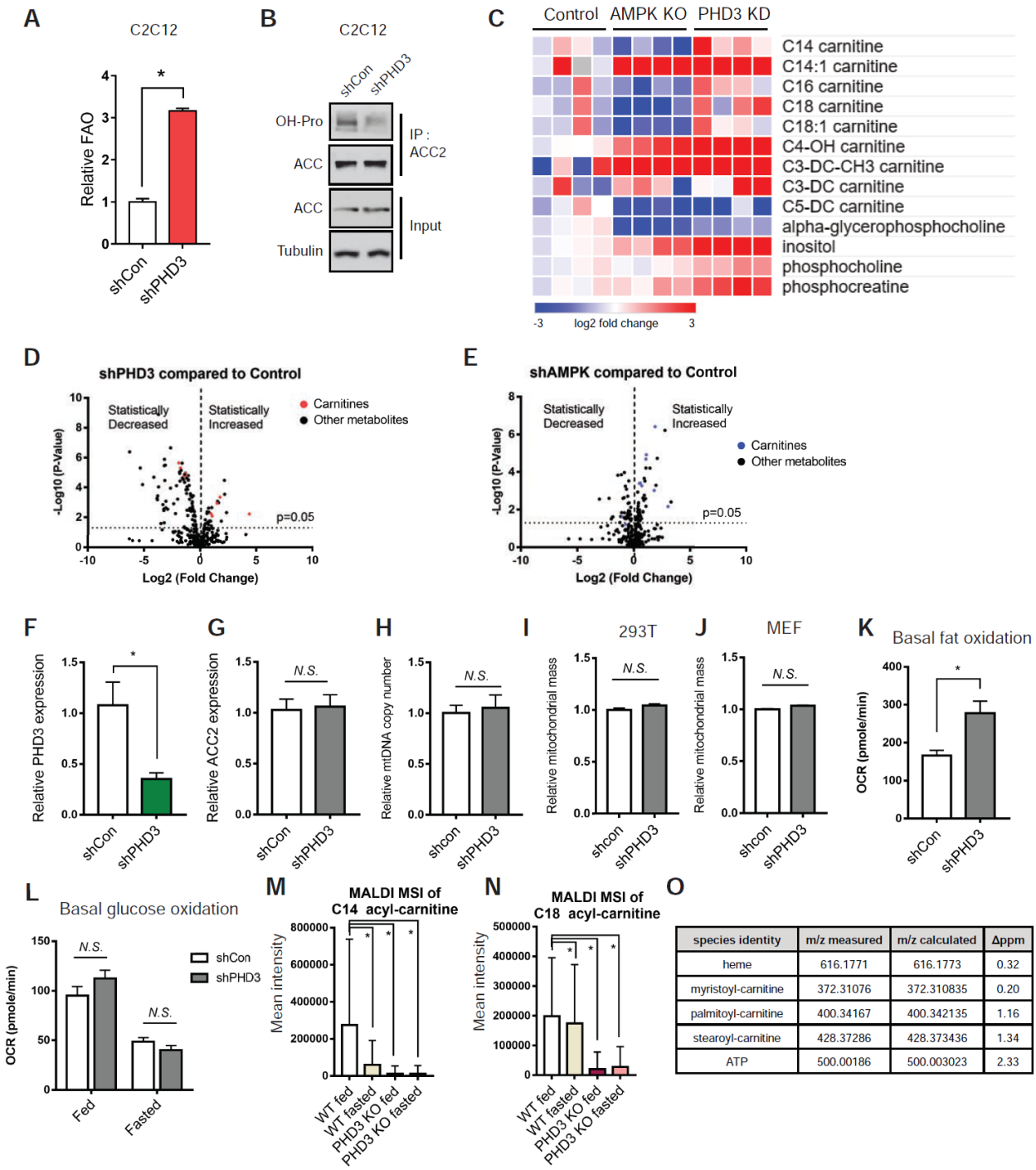

species identity	m/z measured	m/z calculated	Δppm
heme	616.1771	616.1773	0.32
myristoyl-carnitine	372.31076	372.310835	0.20
palmitoyl-carnitine	400.34167	400.342135	1.16
stearoyl-carnitine	428.37286	428.373436	1.34
ATP	500.00186	500.003023	2.33

Figure S4. PHD3 and AMPK have differential functions in fat metabolism, but do not affect mitochondrial biogenesis.
(A) Palmitate oxidation in shcontrol or shPHD3 C2C12 cells using FAO analysis (n=3). (B) Immunoblots of anti-ACC2 immunoprecipates and corresponding whole-cell lysates of shcontrol or shPHD3 C2C12 cells. (C) Heat map depicting metabolite abundance in PHD3 knock-down, AMPKα knock out or non-silencing control MEFs. Volcano plots demonstrating that PHD3 (D) and AMPK depleted MEFs (E) have numerous statistically significant metabolic changes compared to control cells. Red and blue dots indicate each acyl-carnitine. PHD3 expression (F) or ACC2 expression (G) using B2M as a reference gene in shControl or shPHD3 HEK293T cells. (H) Mitochondrial DNA number was not changed by PHD3 knockdown. mtDNA levels were measured by MT-CO2 using human b-actin as a reference gene in shControl or shPHD3 HEK293T cells. Mitochondrial mass of 293T cells (I) or MEFs (J) depleted of PHD3 or control shRNA using MitoTracker Green (n = 5). (K) The basal extracellular acidification rate (ECAR) in shControl or shPHD3 MEFs (n = 15). (L) Basal oxygen consumption rate (OCR) tracing for high or low glucose cultured shControl or shPHD3 MEFs, measured using a Seahorse Bioscience XF24 Extracellular Flux Analyzer (n = 15 wells). Matrix-assisted laser desorption/ionization mass spectrometry imaging (MALDI-MSI) of myristoyl-carnitine (m/z 372.310835, Δppm = 0.2) (M), and stearoyl-carnitine (m/z 428.37286, Δppm = 1.34) (N) in WT or PHD3 KO mouse quadriceps under fed or fasted conditions. (O) Measured and calculated mass of species detected by MALDI MS (FT-ICR MS so <2 ppm expected).

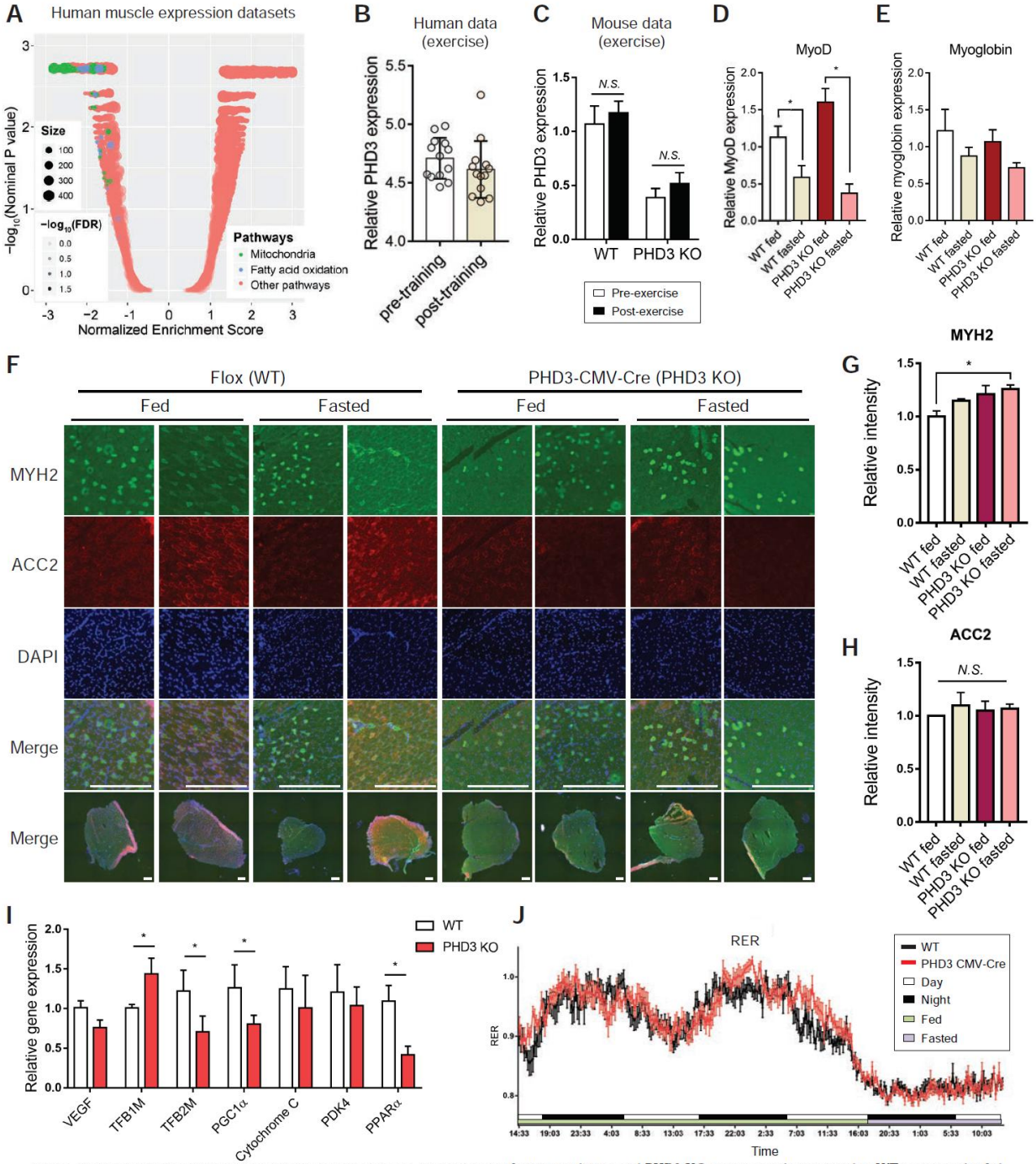

Figure S5. The expression of ACC2 or muscle markers were not changed under fasting conditions and PHD3 KO mouse compared to WT mouse under fed conditions.

(A) Gene set enrichment analysis of PHD3 indicating its negative connection with fatty acid oxidation and mitochondrial pathways in human muscle dataset (GSE3307). Mitochondrial and fatty acid oxidation pathways are highlighted in green and blue, respectively. The size of dot represents the number of genes in the pathway, and transparency indicates the significance (- log10 (FDR)) of the enrichment between this pathway and PHD3 expression. (B) PHD3 expression levels in human muscle biopsies after untraining or endurance exercise training (GSE111551). Data represent means ± SEM. (C) Relative PHD3 expression using mouse beta-actin as a reference gene in WT or PHD3 KO mice quadriceps with exercise (n=9). The mRNA levels of MyoD (D) and myoblobin (E) in WT or PHD3 KO mouse quadriceps under fed or fasting conditions (n = 4). * $p < 0.05$. (F) Immunofluorescence by MYH2, which is Myosin Heavy Chain Type IIA (green), ACC2 (red) and DAPI (blue) in WT or PHD3 KO mouse quadriceps under fed and fasted conditions. Scale is 500 μm. Relative intensity of MYH2 (G) and ACC2 (H). Normalized by relative intensity of DAPI. (I) Gene expression using mouse β-actin as a reference gene in WT or PHD3 KO mouse quadriceps (n = 4). (J) Respiratory exchange ratio (RER) in 20 weeks of WT or PHD3 KO mice using Comprehensive Lab Animal Monitoring System (CLAMS) (n=9). WT or PHD3 KO mice were under fed condition 48 hours and fasted condition 16 hours.

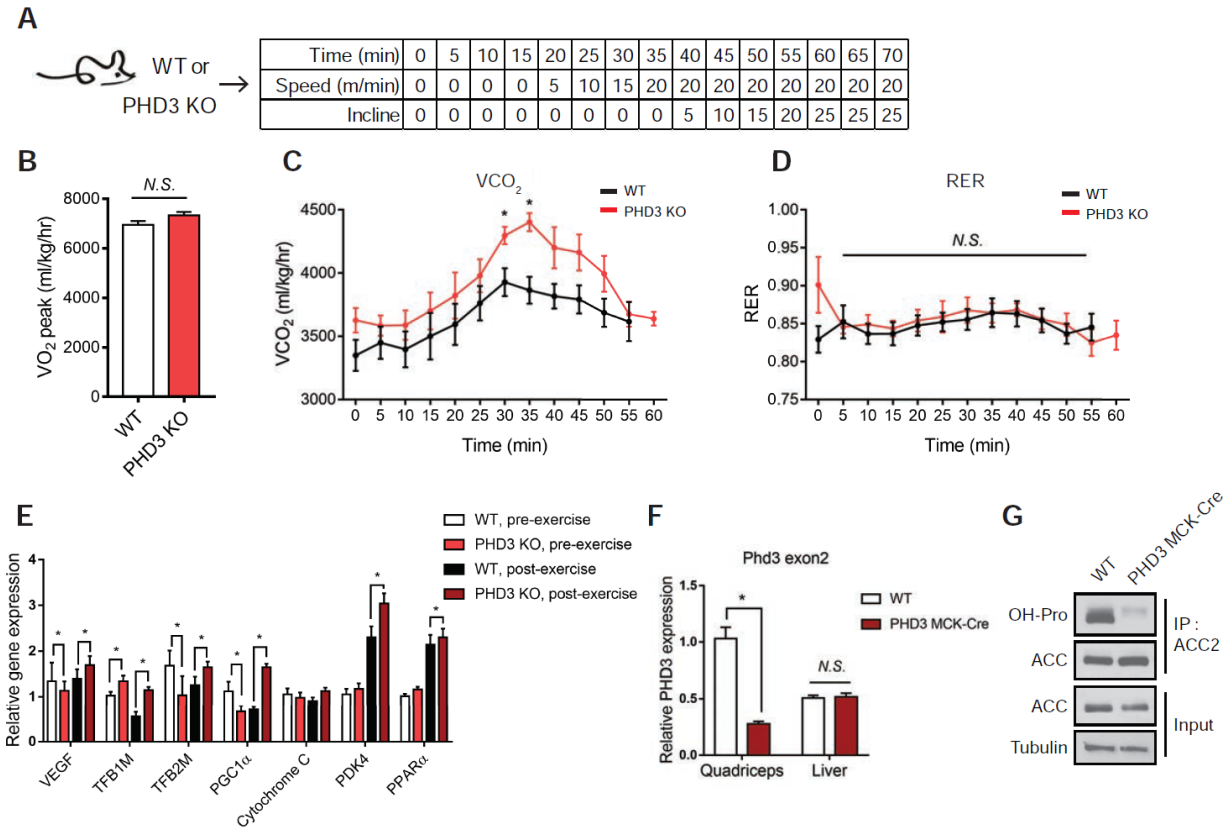

Figure S6. PHD3 KO mice have increased exercise capacity compared to WT.
(A) Schematic of the trademill experiment until mouse exhaustion. (B) Age-matched mice after 20 weeks were individually placed in metabolic cages and allowed to acclimatize for 48 h before readings were taken (n = 8 mice per group). Mean whole-body maximum oxygen consumption rate of both genotypes were calculated from the individual performances. Data represented means ± SEM. *P < 0.05. (C) Mean whole-body CO_2 until exhaustion. (D) RER (VCO_2/VO_2). Data represented means ± SEM. *P < 0.05. (E) Gene expression using mouse β-actin as a reference gene in WT or PHD3 KO mouse quadriceps under pre- or post-exercise condition (n=4). (F) qPCR analyses to confirm the lack of WT mRNA transcripts in WT or PHD3 MCK-Cre KO mouse quadriceps and liver RNA samples. (G) Immunoprecifitation and western blotting analysis of ACC2 hydroxylation in WT or PHD3 MCK-Cre KO mice quadriceps.